Defence Research and Development Canada
Recherche et développement pour la défense Canada

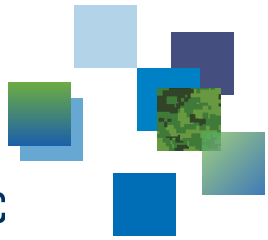

DRDC | RDDC
technologysciencetechnologie

On the use of the force time histories to determine the shock and steady state interface pressures exerted by the impact of a low-strength projectile

D. Nandlall
DRDC – Valcartier Research Centre

A. Gakwaya
Université Laval

Defence Research and Development Canada
Scientific Report
DRDC-RDDC-2018-R161
July 2018

Canada

IMPORTANT INFORMATIVE STATEMENTS

This document was reviewed for Controlled Goods by DRDC using the Schedule to the *Defence Production Act*.

Endorsement statement: This publication has been peer-reviewed and published by the Editorial Office of Defence Research and Development Canada, an agency of the Department of National Defence of Canada. Inquiries can be sent to: Publications.DRDC-RDDC@drdc-rddc.gc.ca.

Abstract

The work presented in this report examines the impact process of a 10% gelatine soft body material projectile striking a rigid target attached to a quartz force ring sensor. Using the shock Hugoniot relations and the conservations equations, a theoretical relation was obtained for the interface shock pressure. The Alekseevskii-Tate penetration equations were used to interpret and determine the steady state pressure applied to the target.

Impact tests were conducted and the time histories of the force applied to the target were measured. The force-time curves were examined to identify frequencies that were present in the results and may be coming from the natural vibrations of the various parts that make up the target. Bessel function solutions for the wave equation applied to the free vibration of plates were used to identify and quantify the frequencies of the various plates in the target assembly. These unwanted frequencies were removed using the Savitsky-Golay filter. The shock pressures were then derived and very good comparison was obtained with the theoretical values predicted by the interface shock pressure equation developed.

The Alekseevskii-Tate equation predicted very well the duration of the interaction between the projectile and the target. However, the measured value of the pressure was in discordance with the expected stagnation pressure, $P_{stagnation} = \frac{1}{2}\rho v_i^2$. In accordance with the Alexseevskii-Tate equation, the results indicate the presence of a dynamic pressure that maybe playing a significant role in the applied steady state pressure. A quantitative measure of this dynamic pressure was obtained.

Significance for defence and security

Low strength materials such as water, gelatine, vulcanization rubber, wax, emulsions or even aluminum foam are used for a broad range of applications involving impact and shock loading conditions. These materials referred to as soft body materials, are not only used in energy absorbing systems but also as surrogate materials for animals, birds and human body tissues and organs. To minimize shock or impact induced effects such as the trauma and damage caused by a projectile impacting human tissue, the interaction of the shock and the subsequent loading caused by the projectile need to be clarified and understood in terms of the propagation of the shock and the role of the ensuing material deformation mechanisms such as strain rate effects and failure mechanisms. This work pushes the boundaries of the methods to characterise these materials and could be useful in designing, developing and testing of protective equipment or structures using soft body material surrogates.

Résumé

L'étude présentée dans ce rapport examine le processus d'impact d'un projectile composé d'un matériel mou de 10% gélatine qui frappe une cible rigide attaché à un capteur de force annulaire. En utilisant les rapports de choc Hugoniot et les équations de conservation, une relation théorique de pression de choc a été obtenue à l'interface entre le projectile et la cible. Les équations de pénétrations d'Alekseevskii-Tate ont été utilisées pour déterminer la pression stationnaire appliquée sur la cible.

Des tests d'impact ont été effectués et les courbes de variation de force contre le temps appliqué sur la cible ont été obtenues. Ces courbes ont été examinés afin d'identifier des fréquences présentes dans les signaux et il est fort probable que ces fréquences naturelles peuvent provenir des différentes parties dont la cible est composée. Les solutions de fonctions Bessel pour l'équation d'onde appliquée à la vibration libre des plaques ont été utilisées pour identifier et déterminer quantitativement les fréquences des différentes plaques dont la cible est composée. Ces fréquences indésirables ont été enlevées en utilisant le filtre Savitsky-Golay. Subséquemment les pressions du choc ont été dérivées et une bonne comparaison avec les valeurs théoriques a été obtenues.

L'équation d'Alekseevskii-Tate a très bien prédit la durée de l'interaction entre le projectile et la cible. Cependant, le valeur de la pression a été en désaccord avec la pression de stagnation $P_{stagnation} = \frac{1}{2}\rho v_i^2$, anticipée. En interprétant les résultats selon les équations d'Alekseevskii-Tate, ces résultats indiquent la présence d'une pression dynamique qui jouerait un rôle signifiant dans la pression de l'état d'équilibre appliquée. Une mesure quantitative de cette pression dynamique a été obtenue.

Importance pour la défense et la sécurité

Matériaux peu résistants tel que l'eau, la gélatine, le caoutchouc de vulcanisation, la cire, les émulsions ou même la mousse d'aluminium ont été utilisés pour une large gamme d'applications impliquant des conditions de choc et d'impact. Ces matériaux, appelés matériaux de corps mous, ne sont pas seulement utilisés dans les systèmes d'absorption d'énergie, mais d'autres sont utilisés comme matériaux de substitution pour les animaux, les oiseaux et les tissus du corps humain et les organes. Pour minimiser les chocs ou les dommages causés par un projectile touchant le tissu humain, l'interaction du choc et le comportement ultérieur causé par le projectile doivent être clarifiés et compris en termes de propagation du choc et du rôle de ces matériaux, tels que le taux de déformation. Ce travail pousse les limites des méthodes de caractérisation de ces matériaux et pourrait jouer un rôle important dans la méthode de conception, le développement et les essais d'équipement et structures de protection.

Table of contents

List of figures

List of tables

Acknowledgements

The author would like to thank all those who helped on this project. In particular, he would like to express his very sincere thanks and gratitude to Dr. Grant McIntosh for the many hours of discussion on impact physics and Bessel functions, without which the author would certainly not have achieved as much detail both from the theoretical methods and experimental analysis. A special thank you to Dr. Sacha Nandlall for introducing the Savitsky-Golay filtering method without which processing the experimental results would have proven much more difficult. Sincere and earnest thanks to Nelson Viel who took our clouded thoughts of a sabot and brought them to reality using additive manufacturing and to Daniel Gautier for the data acquisition. There were many challenges and he made it work. Finally, a very special thank you to Denis Leclerc, a technician of immense skill and knowledge. The experiments worked even better than we thought they would go because we were in uncharted territory launching gelatine projectiles.

1 Introduction

Low strength materials such as water, porous and non-porous gelatine, room temperature vulcanization (RTV) rubber, wax, emulsions or even aluminum foam are used for a broad range of applications involving impact and shock loading conditions. These materials sometimes referred to as soft body materials, are not only used in energy absorbing systems but more so some of these materials such as gelatine or RTV rubber are used as surrogate materials for animals, birds and human body tissues, organs and biological liquids. In recent years in the medical domain, shock waves have been use for various applications and one of the most successful examples is the non-invasive disintegration of unary tract stones using extra-corporeal shock wave lithotripsy. Other examples of the shock loading of soft body materials or soft body impacts include insects hitting an automobile windshield, birds striking an aero-engine or aircraft fuselage, ice particles impacting structures at high velocities, snowballs falling on windows or a bullet striking and penetrating animal or human tissue or even a lead bullet striking a steel target. During the impact of a soft body onto a hard target such as an aircraft structure, the soft material is highly deformable and tends to flow over the target. In the case where the target is the soft body and the impactor is hard body, such as a bullet for example, the soft body material will flow over the hard impactor. In all cases the soft body material will flow if the generated stress during impact greatly exceeds its yield strength.

To minimize shock or impact induced effects such as damage to an aircraft structure from a bird impact or the trauma and damage caused by a projectile impacting human tissue, the interaction of the shock and the subsequent loading caused by the projectile need to be clarified and understood in terms of the propagation, reflection of the shock and the role of the ensuing material deformation mechanisms such as strain rate effects and failure mechanisms. From the point of view of understanding the impact and dynamic response of these soft body materials, in addition to performing experiments, physics based numerical simulations of the impact and/or shock loading problem could prove extremely useful and meaningful. However, to conduct these simulations the numerical schemes require reliable material physical properties such as the constitutive properties, shock data or equations of states and these are often obtained from carefully developed and validated experimental methods.

1.1 Objective

In the examination of the impact of a soft body onto a target the shock and the steady state pressures are parameters that are important in determining both the projectile and target response. These parameters are normally measured at the projectile/target interface. To measure these properties, many researchers have often used pressure transducers embedded in the target surface where the projectile strikes the target. However, in all the work cited although good results were obtained they were many difficulties, such as the limitation of the pressure gauges, that rendered sometimes the accuracies of the data being questionable. These include resonance frequencies that cause noise to appear or the gauges not having a

fast enough response time to capture the fast rising edge due to especially strong shocks. In fact Wilbeck [1], Lavoie [2], Heimbs [3], Hedayati and Sadighi [4], to name a few, all highlighted these limitations and this led the authors to re-look at issues of the impact problem and examine whether the shock and steady state parameters could be obtained more precisely.

Thus, given the foregoing discussion, the objectives of this work were threefold. Firstly, using the shock Hugoniot relations and the conservation equations, develop a relation for the interface shock pressure and further to that, examine whether the Alekseevski-Tate penetration equations could be applied to determine the steady state impact parameters. Secondly, using a soft body projectile impacting a rigid target, investigate the feasibility of using a force transducer as the rigid target to capture the force-time response at the interface and then from that history examine whether or not the shock and steady state pressures could be extracted. Thirdly, to interpret and compare the experimentally deduced shock and steady state pressures with the theoretical values determined in accordance with the shock Hugoniot relations and the Alekseevskii-Tate penetration equations.

1.2 Theoretical background

Most researchers [1–27] will agree that for most impact problems the mechanisms that govern the impact process are very dependent on the striking velocity. With regards to low strength materials, the 1978 literature and theoretical review provided in the work of Wilbeck [1] and Barber, Taylor and Wilbeck [4, 5, 6] on the impact of low strength materials still remain very relevant today because of the basic description of the impact process and extensive experimental data available for a variety of bird surrogate materials striking rigid targets. They define the very basic physical impact phenomena that occur with these types of problems. The review conducted by Hiembs [2] includes a copious list of studies on the subject of soft body impact and complements very well the modelling advances made in simulating these types of impact while the recent text by Hedayati and Sadighi [3] covers very well, albeit from an engineering standpoint, advances made in modelling and experimental methods for examining the problem but focusing on the bird impact problem. In a 2009 series of tests, Lavoie et al [7,8] attempted to measure the shock and steady state interface pressures of gelatine projectiles striking an instrumented solid target and for many reasons described by Hedayati and Sadighi [3] much discrepancies between the analytic, numerical and the experimental results were found. In a 2014 study, Liu et al [9] carried out bird impact experiments to guide and conduct numerical analysis of the problem but no shock nor steady state interface pressures were measured or presented. Given the foregoing discussion, it seems necessary to revisit the problem and the basic impact phenomena involved and investigate if there is a way to measure the interface parameters from simple impact experiments.

Hopkins and Kolsky [10] in their 1960 study of impact of solids defined five regimes of the impact process depending on the striking velocity. These are the elastic impact, the plastic impact, the hydrodynamic impact and the explosive impact. In an elastic impact the stress

waves generated in the projectile or target do not exceed the strength of the materials and thus, the response of the impact depends only on the elastic moduli and the elastic wave velocities of the materials. As the impact velocity is increased a plastic impact occurs where the stresses produced cause the material to deform plastically. In this case the material strength is the governing factor of the response. As the impact velocity is further increased the stresses generated by the deceleration of the material on impact greatly exceeds the yield strength of the material and it starts to flow. In this hydrodynamic regime, the material can be treated as a fluid for all intent and purposes and in this case it is the material density and not the strength that dominates the response of the impact. In all the regimes described stress waves propagate through the projectile and target. As the impact velocity is increased and the velocity of the stress waves exceeds the characteristic wave or acoustic velocity of the material, more energy is dissipated in the local region of the impact area. Shock waves are now generated and the wave motion begins playing an increasingly important role in the determination of the local stress distribution. The heat produced in the impact zone is concentrated in this very small region and can be sufficient to melt or vaporize the material. Hopkins and Kolsky [10] explains that the impact process in this regime is very analogous to a small explosion occurring or taking place on the surface of the target. Although these regimes have been defined very well for high strength materials interaction there is no reason not to believe that these regimes are also applicable to low strength materials as pointed out by Barber, Taylor and Wilbeck [1,3,4,5] in their study of the characterization of bird impact on a rigid plate. When the stresses generated during impact greatly exceed the yield strength of the material, the problem can be approached hydro-dynamically This is because strength and viscosity have very little effect on material response and rather, it is an equation of state relating the pressure, density and energy that should be used to study or describe the material response. A very good example of this is given by Hopkinson [11] in the studying of the impact of a lead bullet onto a steel target in which he found experimentally that the stresses generated in the projectile by the impact could be approximated with a fluid jet impacting the target. Other researchers such as Birchoff [12], Heymann [13], Johnson and Vickers [14] to name a few, have also confirmed this in their studies of high speed impact of water drops and jets impacting solid surfaces. In all these investigations, there are several features of the impact process that are of importance. Heymann [13] in fact, explained that these are the initial pressure, the area over which the pressure is exerted, the lateral velocity of the material flow after impact and the decay time of the impact forces.

A major hurdle in the area of soft body impact is that the stresses generated at the projectile/target interface could be so large that the target would also experience very large deformations especially if the target is either thin or comprises of soft materials. This simultaneous large deformation of both the projectile and target makes uncoupling the target response from that of the projectile very difficult. To decouple the soft body projectile response, many researchers [1,4,5,7,8] have studied the impact of soft body cylinders on rigid targets. Bowden and Brunton [15,16] in extensive studies of the deformation of solids by liquid impact at supersonic speeds examined the impact of a flat-ended cylinder on a rigid target and described the interface pressure as the water hammer pressure, $P = \rho c_0 u_0$

where ρ is the density and c_0 is the wave speed and u_0 is the impact velocity. Bowden and Field [17] in a later work on the investigation of impact of liquids and solids on rigid targets explains that the water hammer equation of the pressure works only for low velocity impact but for higher impact velocities the wave velocity, c_0, must be replaced by the shock velocity, U_s, to give the true interface pressure. Many researchers have since validated this theory and in fact, Glen [18] with his investigation on the dynamics of hypervelocity impact of liquid jet impacting a rigid flat surface, has shown that the peak pressure at the surface or interface is the shock pressure or Hugoniot pressure given by $P_i = \rho U_s u_0$ where U_s is the shock speed. Once the release waves have propagated into the center of the cylinder the pressure begins to decrease. After several reflections, the flow of the projectile will approach a steady state condition. The steady state pressure at the center of the projectile is the stagnation pressure given by $P_{stagnation} = \frac{1}{2}\rho u_0^2$, determined from Bernoulli's equation for steady state flow for an incompressible fluid. The work of Glen [18] confirmed these observations made by Cook [19] and Heymann [13] who actually identified these two basic regimes of water jet impact; the shock regime which is governed by the Hugoniot pressure and steady flow regime governed by the stagnation pressure; there is general agreement on this interpretation from the cited literature.

However, with regards to the characterization of soft body material impact, there are many researchers who have made many contributions but the original work by Wilbeck [1] and Barber et al [4,5,6] still stand out and are used extensively mostly in part because the work provides large experimental data in addition to the basic hydrodynamic theory that describes impact of soft body projectiles striking a flat rigid plate.

2 Determination of the interface shock pressure and speed from the shock Hugoniot relations

Figure 1 describes the four phases of the impact of a soft body projectile striking a rigid target. Figure 1(a) shows the initial contact made by the projectile with an impact velocity of u_0. Assuming that the projectile is moving from left to right, a left hand moving shock is generated in the projectile whereas a right hand moving shock is generated in the target. With regards to the projectile, the left hand going shock leads to a significant pressure gradient between the outside surface of the projectile and the center causing the outward flow of the material as a release wave moves towards center of the projectile as illustrated in Figure 1(b). After several reflections of the release waves the material flows steadily as depicted in Figure 1(c). At this point the pressure at the center of the projectile is no more the shock pressure but is at a steady state and is known as the stagnation pressure. The material continues to flow until the projectile has essentially completely eroded away as shown in Figure 1(d).

When a shock is generated, the shock front in the material moves with a velocity U_s which is material dependent. The material behind the shock front moves with a particle velocity, u_p. For an impact problem, simply stated, a Hugoniot is a curve that contains all possible equilibrium states at which a material can exist when shock loaded at different impact velocities. It is in fact, an empirically derived curve that relates any of the following variables to each other: the shock pressure, P_s, the shock and particle velocities, U_s and u_p, respectively, and ρ, the shock density. The Hugoniot is not an equation of state, although it could be used in a similar manner and is sometimes used as an isentrope, even though strictly speaking it is not because entropy does increase across the shock front. The Hugoniot is normally derived experimentally where in the simplest case, the velocity Hugoniot, often referred to as the $U_s - u_p$ curve, is an empirical relationship that relates the shock front velocity, U_s, with that of the particle, u_p. Experiments have shown that for most materials it is a simple linear relationship that is expressed in the form

$$U_s = c_0 + s u_p \tag{1}$$

where c_0 is sometimes called the bulk sound speed but is also the intercept on the U_s axis, and s is the particle velocity coefficient obtained experimentally. Figure 2 shows the $U_s - u_p$ curve for gelatine where $c_0 = 1445\ m/s$ and $s = 1.9$. These experimental values are taken from Gojani et al [20] and are presented in Table 1 along with similar values for the steel target.

The real power of Equation (1) comes when it is used in conjunction with the equations of conservation of mass, momentum, and energy. The three equations, Equations (2) to (4) taken from Cooper [21] are given below, respectively, for the mass, momentum and energy.

$$\frac{\rho_1}{\rho_0} = \frac{\nu_0}{\nu_1} = \frac{U_s - u_0}{U_s - u_1} \tag{2}$$

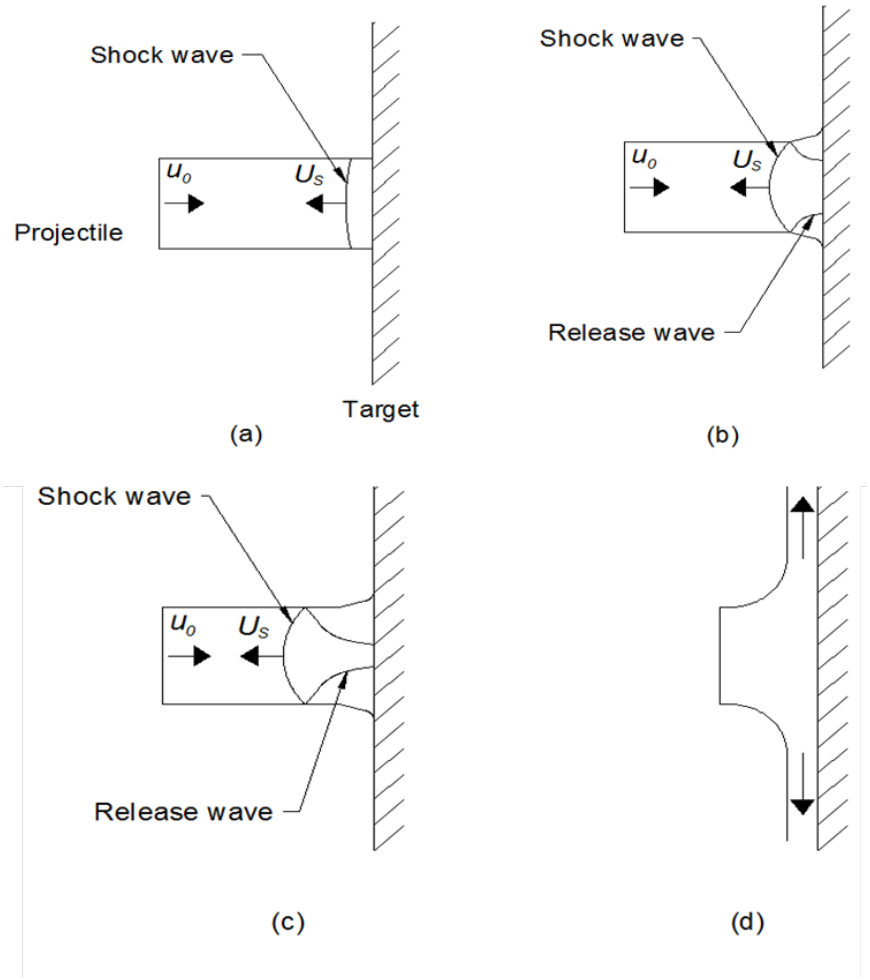

Figure 1: *Illustration of the four stages of a soft body projectile striking a rigid target.*

$$P_1 - P_0 = \rho_0 \left(u_1 - u_0\right)\left(U_s - u_0\right) \tag{3}$$

$$e_1 - e_0 = \frac{\left(P_1 u_1 - P_0 u_0\right)}{\rho_0 \left(U_s - u_0\right)} + \frac{1}{2}\left(u_1^2 - u_0^2\right) \tag{4}$$

where the subscript "0" is for conditions ahead of the shock front and "1" is for after the shock wave has passed. Equations (1) to (4) can be applied to all materials under shock loading conditions. Now, consider the impact problem described in Figure 1 with the projectile moving from left to right for convenience. Following the derivation set out in Cooper [21] and Carlucci et al [22] to describe the shock pressure for the right going shock in the target, that is for $u_p > u_0$, combining Equation (1) with Equation (3), the momentum equation, and rearranging the terms to make the pressure, P, the subject of the equation and as a function of the material velocity u, the following $P - u$ Hugoniot is obtained.

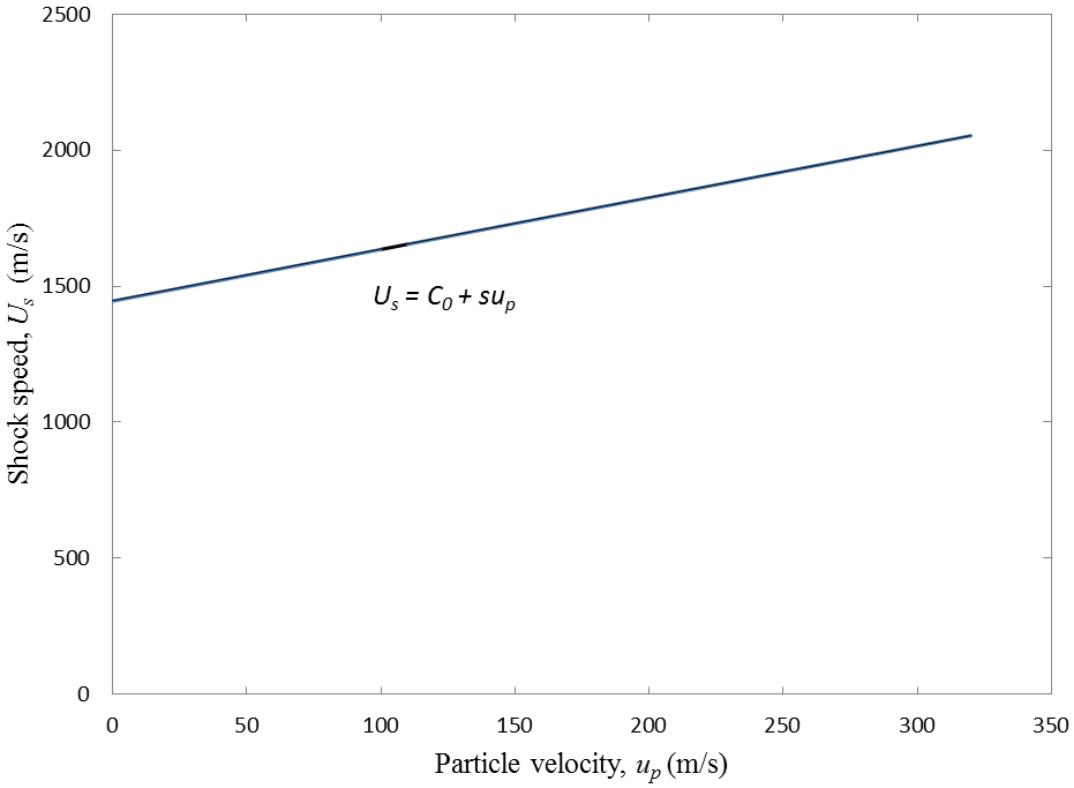

Figure 2: *The shock velocity – particle velocity or $U_s - u_p$ curve for 10% gelatine using parameters taken from Gojani et al [20].*

$$P_{1t} = \rho_{0t} c_{0t} \left(u_{1t} - u_{0t}\right) + \rho_{0t} s_t \left(u_{1t} - u_{0t}\right)^2 \tag{5}$$

where the subscript t relates to the properties of the target material. For the left going Hugoniot, that is for $u_p < u_0$, the shock pressure equation would be given by

$$P_{1p} = \rho_{0p} c_{0p} \left(u_{0p} - u_{1p}\right) + \rho_{0p} s_p \left(u_{0p} - u_{1p}\right)^2 \tag{6}$$

where the subscript p relates to the properties of the projectile material.

As in the case shown in Figure 1, when a projectile impacts a target the following conditions must apply. The pressure must be consistent across the interface and the velocity of the particles of both materials at the interface must be the same to satisfy the conservations equations. These conditions essentially corresponds to solving Equations (5) and (6)simultaneously to determine the interface particle velocity and the shock pressure. Using

Table 1: *Materials properties for gelatine (Gojani et al [20]) and steel.*

Property/parameter	Gelatin	Steel
Density, ρ (kg/m^3)	1030	7800
Acoustic velocity, c_0 (m/s)	1445	5800
Shock parameter, s	1.900	1.434

the parameters shown in Table 1, solving these two equations could be done graphically by plotting the two pressures obtain from the two equations as a function of chosen particle velocities. This is shown in Figure 3 where the shock pressure and the corresponding particle velocity is indicated by the point marked X where the two graphs intersect. It is essential to note here that for the left hand Hugoniot the pressure increases as the particle velocity is decreased. This is because the initial velocity was not changed so it simply means that just before impact the projectile's velocity is suddenly decreased to produce the reduced particle velocity so the amount by which the projectile's velocity has been reduced manifests itself as an increase in the pressure. The case where the particle velocity is zero indicates that the projectile arrives with an initial velocity and essentially abruptly stops just before striking the target thus the pressure is maximum in the projectile but zero at the target.

A more elegant way of determining the shock pressure and the particle velocity that exist at the interface is to equate the left-going Hugoniot, Equation (5) to the right-going Hugoniot, Equation (6). Equating these two equations and eliminating the pressure terms results in a quadratic equation as a function of the common particle velocity, u and could be written as

$$\begin{aligned}\left(\rho_{0p}s_p - \rho_{0t}s_t\right)u^2 - \left(\rho_{0p}c_{0p} + 2\rho_{0p}s_p u_{0p} + \rho_{0t}c_{0t} - 2\rho_{0t}s_t u_{0t}\right)u + \\ \left(\rho_{0p}c_{0p}u_{0p} + \rho_{0p}s_p u_{0p}^2 + \rho_{0t}c_{0t}u_{0t}u_{0t} - \rho_{0t}s_t u_{0t}^2\right) = 0\end{aligned} \tag{7}$$

The positive root of the Equation (7) gives the particle velocity at the interface with the other root being meaningless. Substituting for the particle velocity in either Equation (5) or (6) not only gives the Hugoniot pressure at the interface but importantly also that now the particle velocity is known, the shock speed could be obtained from Equation (1).

Equation (3), the momentum equation, could also be used to obtain the interface shock pressure, P_s, directly by setting the initial pressure, $P_0, = 0$ and $u_{0t} = 0$ to obtain

$$P_s = \rho_{0p}U_s u_{0p} \tag{8}$$

where U_s is the shock speed and u_{0p} is the projectile impact velocity. What is important here is that once the shock speed is known it is simple to calculate the Hugoniot pressure from Equation (8). Using the target and projectile parameters shown in Table 1, Figure 4 shows the variation of the interface shock pressure as a function of the impact velocity for the gelatine projectile striking the rigid target described in Figure 1.

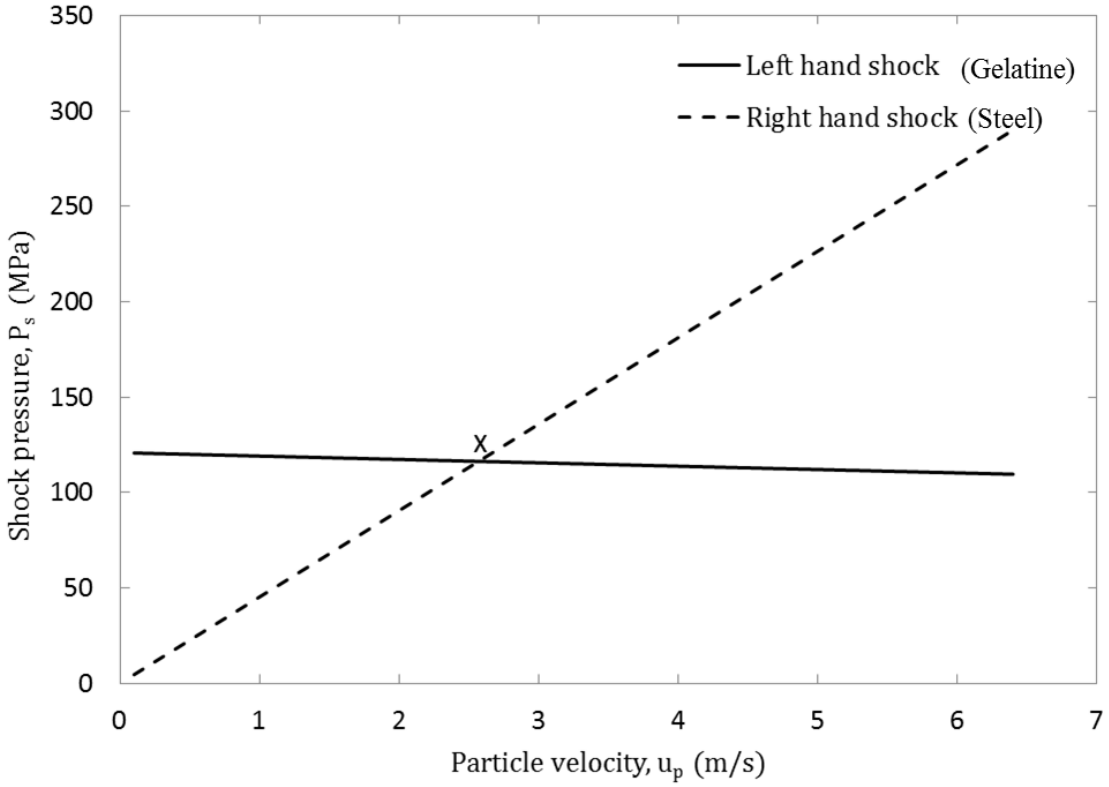

Figure 3: *Right and left hand shock pressure as a function of the particle velocity – $P_s - u_p$ curve.*

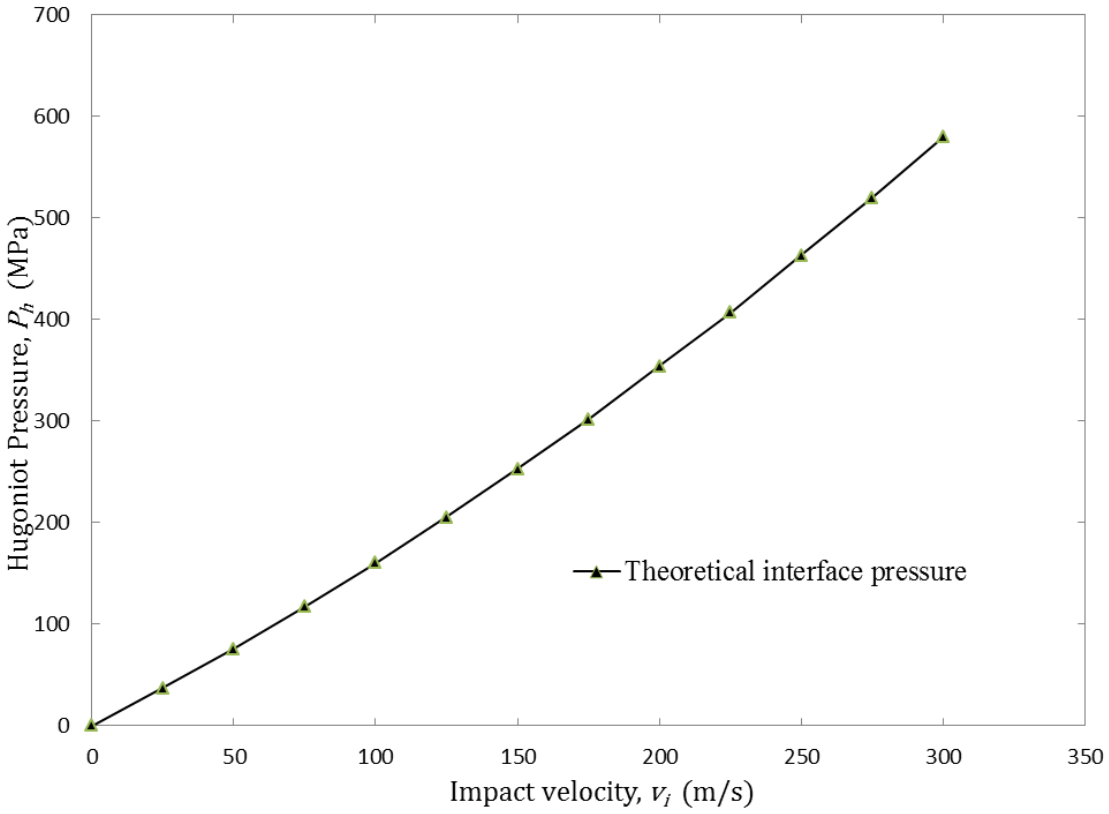

Figure 4: *Variation of the interface shock pressure as a function of the impact velocity.*

3 Development of the steady state pressure from the Alekseevskii-Tate penetration equations

In the 1960s Alekseevskii [23] and Tate [24] independently framed and formulated the penetration equations that describe the behaviour of a long rod penetrator while it penetrates a target at high velocity. These equations are given by

$$l\frac{dv_i}{dt} = \frac{-Y}{\rho_r} \tag{9}$$

$$\frac{1}{2}\rho_r\left(v_i - w)^2\right) + Y = \frac{1}{2}\rho_t w^2 + R \tag{10}$$

$$v = w - \frac{dl}{dt} \tag{11}$$

$$\frac{dP_n}{dt} = w \tag{12}$$

where v_i is the rod velocity, w is the penetration velocity, P_n is the penetration, l is the penetrator length, t is the time after impact, R_t is the target strength and Y_p is the penetrator strength. ρ_p and ρ_t are, respectively, the penetrator and target densities. These equations have been used over the decades to predict the penetration, penetration velocity, rod velocity and they have been integrated numerically by many researchers to give a solution to the penetration problem. A very interesting description of these equations is given by the work of Walters and Segletes [25] who developed an exact solution for these equations. The solution was further refined by Segletes and Walters [26] but these exact solutions yielded the penetration of the target as an implicit function of time. Walters and Williams [27] reexamined the solution to the Alekseevskii-Tate equations and an explicit perturbation solution for the penetration as a function of time was obtained. The results compared very well with the exact numerical integration of the equations and the implicit solution developed earlier. Three special conditions were identified and these are when the target strength is very small or negligible to that of projectile and the penetrator penetrates the target without much erosion of itself. Secondly, in the case where the target strength is the same as the projectile strength a simple close form solution exists and the penetration could be calculated exactly. The third case considers that the projectile strength is negligible compared to that of the target. In this case the projectile erodes way without penetrating the target. This is essentially the case that is presented in the problem of a soft body striking a rigid target. More recently Flis [28] modified the Alekseevskii-Tate equations for rod penetration into porous targets and obtained very good results when compared to experiments. As a result there seems to be very reasonable arguments that these equations could be applied to the soft body impact problem at hand.

Equation (11) could be solved explicitly for the projectile erosion given that the penetration velocity, w is 0. Therefore,

$$\frac{dl}{dt} = v_i \tag{13}$$

which implies essentially that the projectile erosion rate, $\frac{dl}{dt}$ is simply equal to impact velocity, v_i and the flow of the material at the target/projectile interface is considered to be steady state. Performing this simple integration and rearranging the equation making t the subject of the formula simply gives

$$t = l/v \tag{14}$$

which is the time the projectile spends interacting with the target before being completely eroded. Equations (9) and (12) are not required given that the penetration velocity is 0.

In Equation (10), setting the penetration velocity and taking the pressures as the usual strength terms, as is done in Flis [28], the following equation is obtained

$$P_{interface} = \frac{1}{2}\rho_r v_i^2 + Y \tag{15}$$

In the context of the case where the projectile strength is negligible with respect to that of the target, that is $Y = 0$,

$$P_{interface} = \frac{1}{2}\rho_p v^2 \tag{16}$$

is obtained where $P_{interface}$ is referred to as the steady state stagnation pressure, $P_{stagnation}$, that is often found in literature [1–27].

4 Experiments—Description, arrangement and impact tests

4.1 Experimental facility

An air gun impact facility, shown in Figure 5, was used to conduct the experiments.

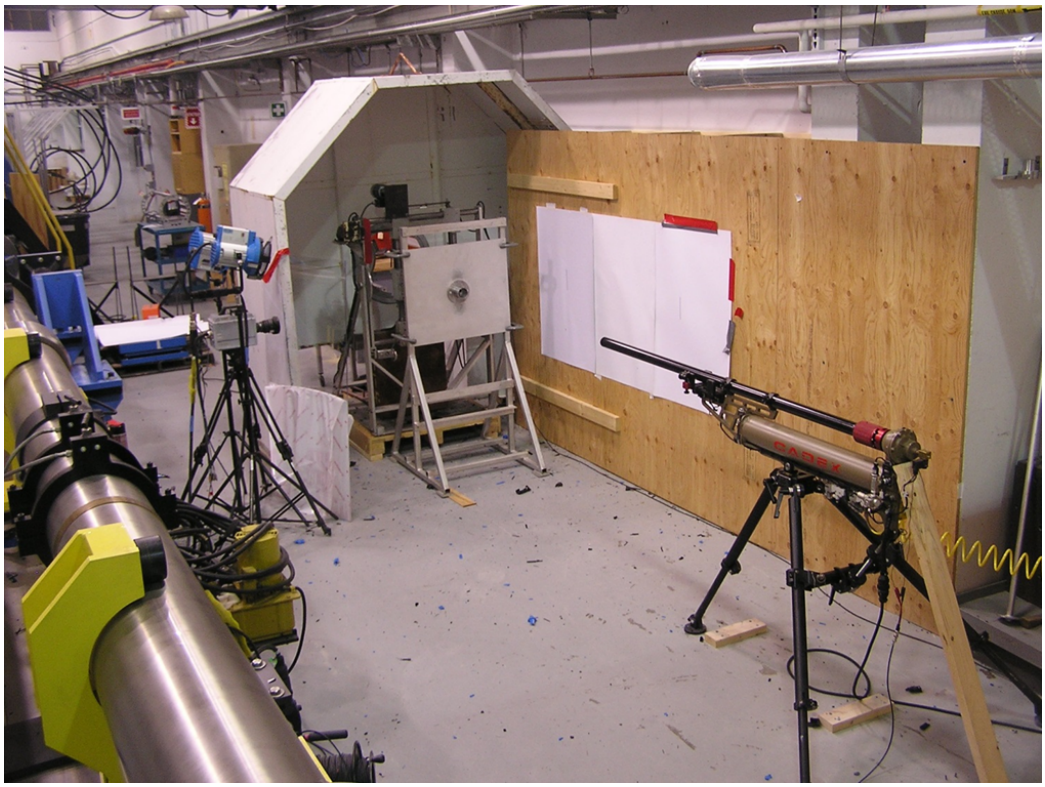

Figure 5: *DRDC's air gun impact facility.*

The air gun itself consists of an 1.8-m long, 40-mm diameter launch tube coupled to a compressed air reservoir located below the launch tube. Coupling of the launch tube with the reservoir is done via a mechanical valve which when opened releases the compressed air which then directly pushes the projectile along the barrel. The pressure in the reservoir determines the exit velocity of the projectile. At this time the maximum reservoir pressure that could be used is 825 kPa (120 psi). A Photron high speed camera (Model SA-5 and SA-1) recording at 20000 frames/s, was used to record the projectile release from the launch package, its flight to the target and the projectile interaction with the target. The data acquisition system, Genesis (Model 5-E), was used to trigger the camera and acquire the force history data.

4.2 Projectile, sabot and target description

To launch projectiles with the air gun, a sabot is required mainly because the diameter of the penetrator is smaller than that of the launch tube. The sabot is, therefore, a structure that holds the penetrator in place during its travel in the launch tube. Figures 6 (a), (b) and (c) show, respectively, the inside and outside views of the sabot and the placement of the projectile in the sabot. The sabot is separated from the penetrator after it exits the muzzle of the gun and is trapped or stopped by what is known as a sabot trap, shown in Figure 6 (d). The projectile passes through the opening in the sabot trap and then continues on towards the target.

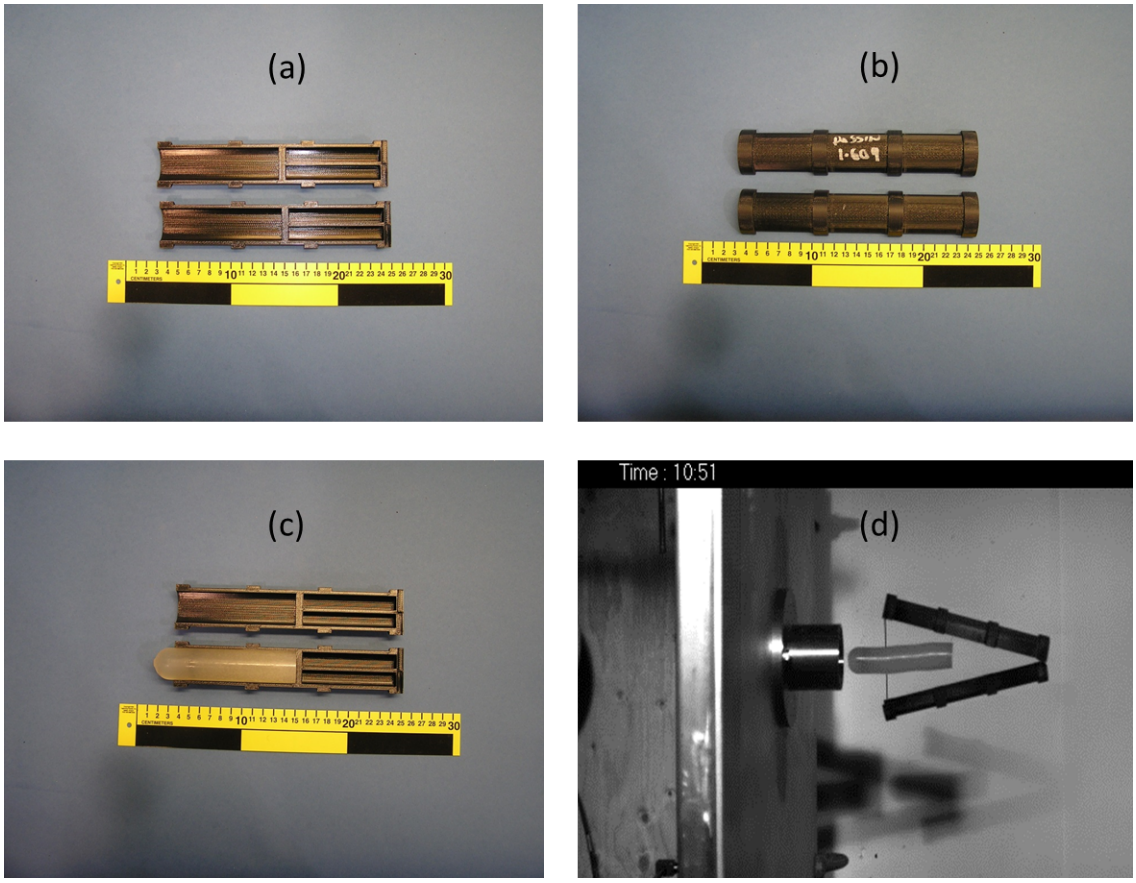

Figure 6: *Various configuration views of the sabot: (a) Outside view (b) Inside view (c) View with the projectile placed in the sabot and (d) the separation of the projectile from the sabot just before passing through the sabot trap.*

Figure 7 shows an typical example of the projectile used for the experiments. The basic projectile used for the tests was a 28-mm cylindrical gelatine rod with a hemispherical tip and a nominal length of 102 mm. It was made from 10 % ballistic gelatine prepared using the recipe taken from Lavoie et al [9].

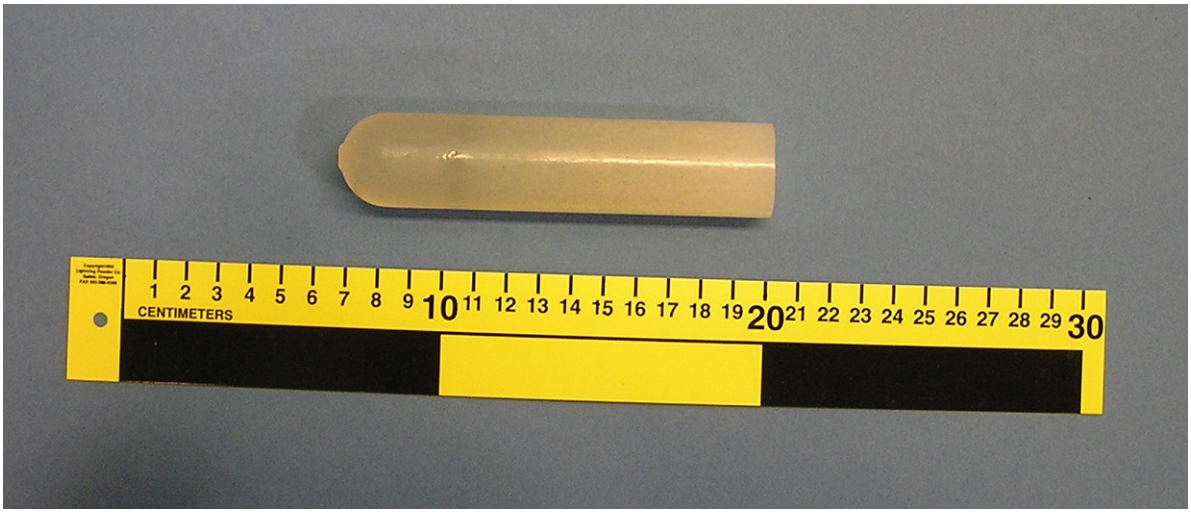

Figure 7: *View of a typical 10% gelatine projectile. In this example the length of the projectile is 130 mm whereas for the test results presented the length of the projectile used was 102 mm.*

To record the interaction between the projectile and target, a PCB Piezotronics Quartz Force Ring Sensor Model 207C with a force measurement range of up to 445 kN was used. Figure 8 (a) shows the ring load cell with a description of its basic characteristics. Figure 8 (b) shows the configuration in which the ring load cell was used. It was sandwiched between two plates, the target disc and the support plate and was pre-constrained to 55000 N as recommended by the manufacturer. This force load cell assembly was then clamped onto the square plate of the target structure, as shown in Figure 9. The whole assembly was then placed behind the sabot trap with the target disc in line with the barrel of the air gun as shown earlier in Figure 5.

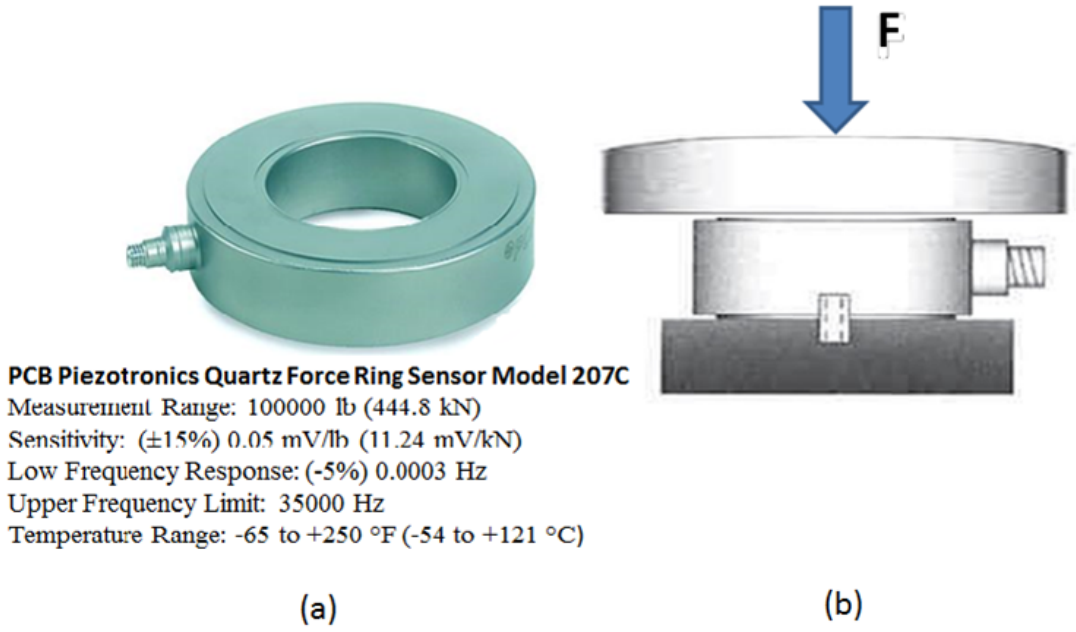

Figure 8: *The Piezotronics Quartz Force Ring Sensor and sketch of its configuration within the target.*

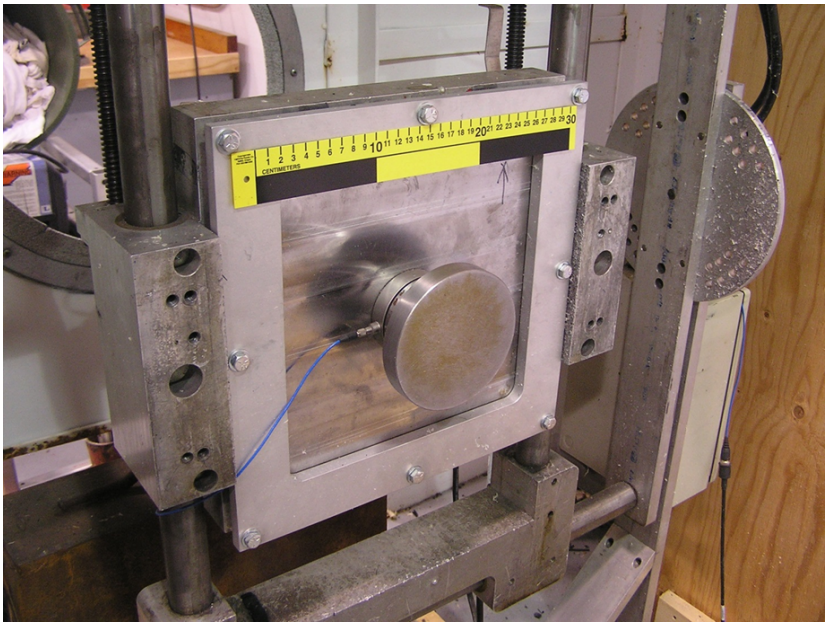

Figure 9: *Experimental target setup.*

4.3 Experimental data reduction and analysis

Many tests were conducted during the course of the experiments where four tests representing different reservoir pressures were chosen to conduct the analysis. These four reservoir pressures produced four impact velocities ranging between 75 to 119 m/s the maximum velocity range that could be obtained from the air gun for the mass of the launch package used. Table 2 shows a summary of the results obtained from the four tests conducted and include the various projectile and gun parameters used to conduct the tests.

Table 2: *Projectile launch parameters, impact velocity and maximum force measured.*

Launch Package (Projectile/Sabot) mass (g)	Projectile length (mm)	Gun pressure (kPa)	Impact velocity (m/s)	Maximum measured force (kN)
64.78/87.63	102.3	275	74	4.79
65.40/87.64	102.8	550	105	11.15
64.98/87.72	102.0	686	115	12.79
65.34/95.10	102.5	818	119	16.47

Figure 10 shows a sequence in time of the projectile/target interaction starting with the projectile striking the target until it was, as in this case, completely eroded. The impact velocity was 119 m/s. A closer look at the sequence of pictures reveals that the eroded material that flows away from the target was made up of small shredded fragments of gelatine. Figure 11 shows some of the shredded fragments collected from the 119 m/s impact velocity test. The significance of these fragments would indicate that the strength of the 10% non-porous gelatine, even though small, of the order of 10 to 50 MPa, compared to the shock pressure of about 200 MPa, does appear to play a role in the steady state pressure applied to the target. This aspect is discussed further below.

Figure 12 shows the force/time histories for the four tests. Examining these force curves, it could be observed that there may be some unwanted high frequencies present that are contributing to the actual force signal. It could also be observed that these high frequency oscillations appear to influence the signal as the impact velocity was increased and thus may need to be removed especially if they are not due to the projectile but rather from the structural response of the target.

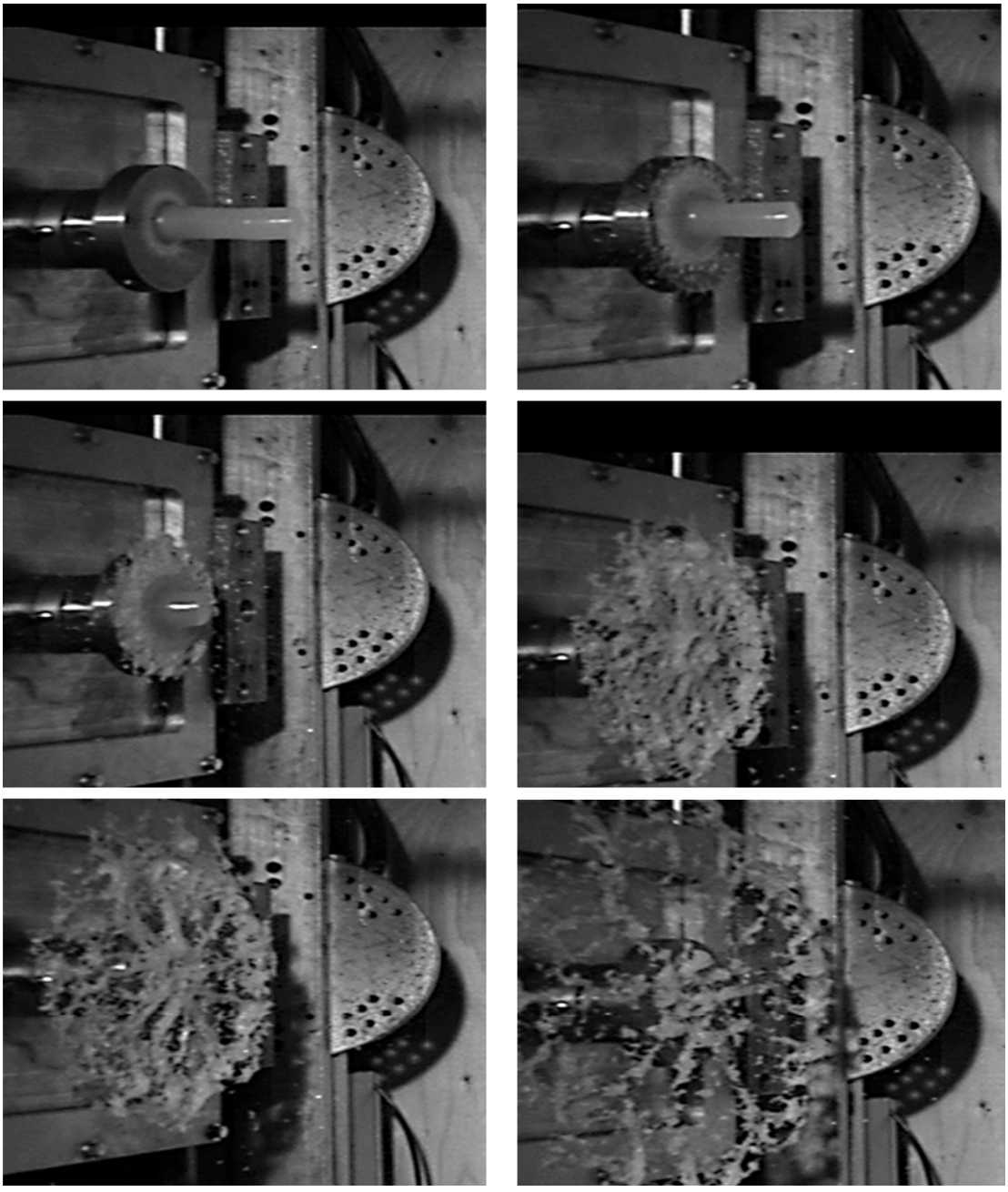

Figure 10: *Time sequence snapshots of the projectile/target interaction for the 119 m/s impact velocity test case.*

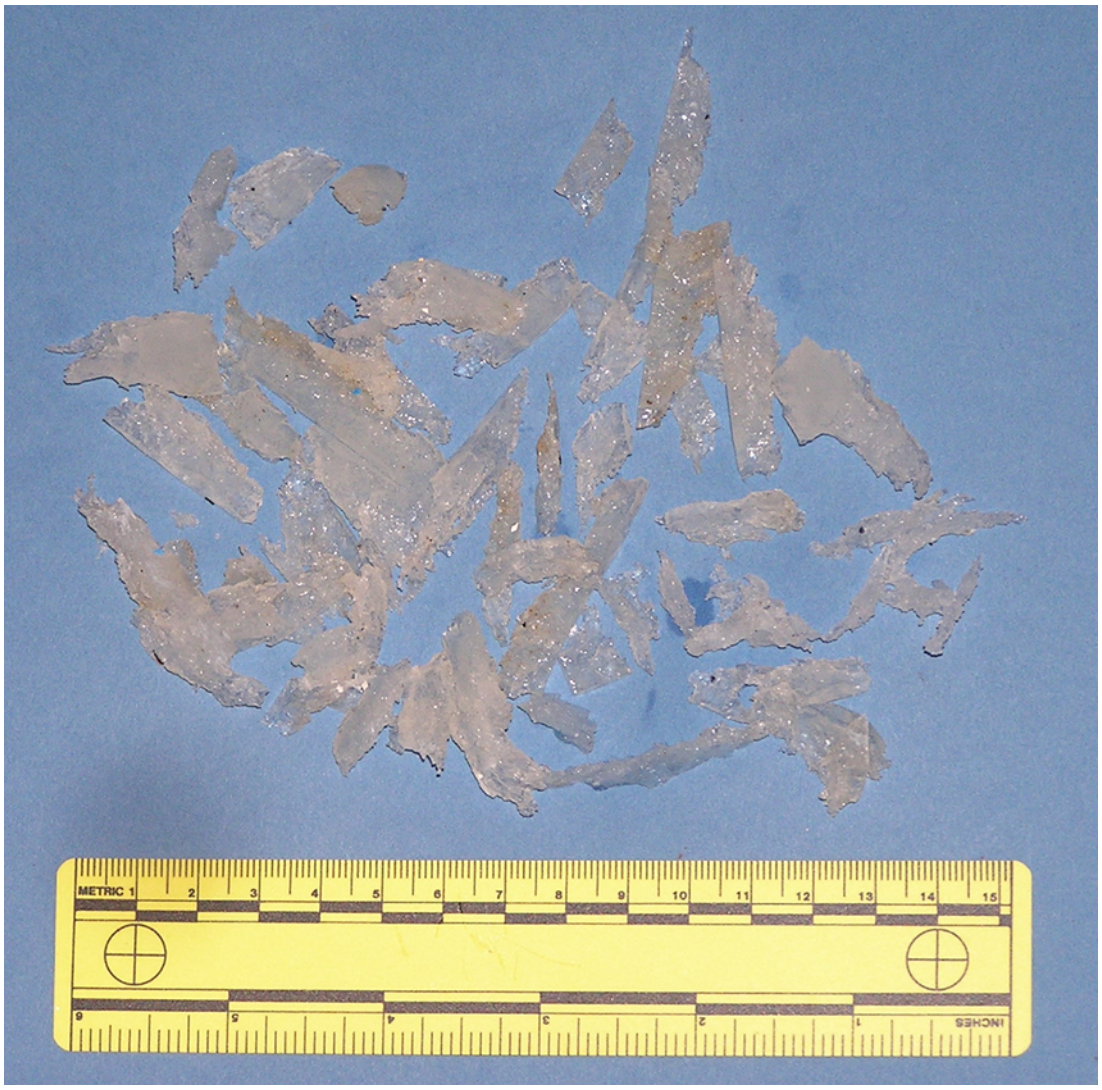

Figure 11: *A collection of shredded gelatine fragments from the 119 m/s impact velocity test case.*

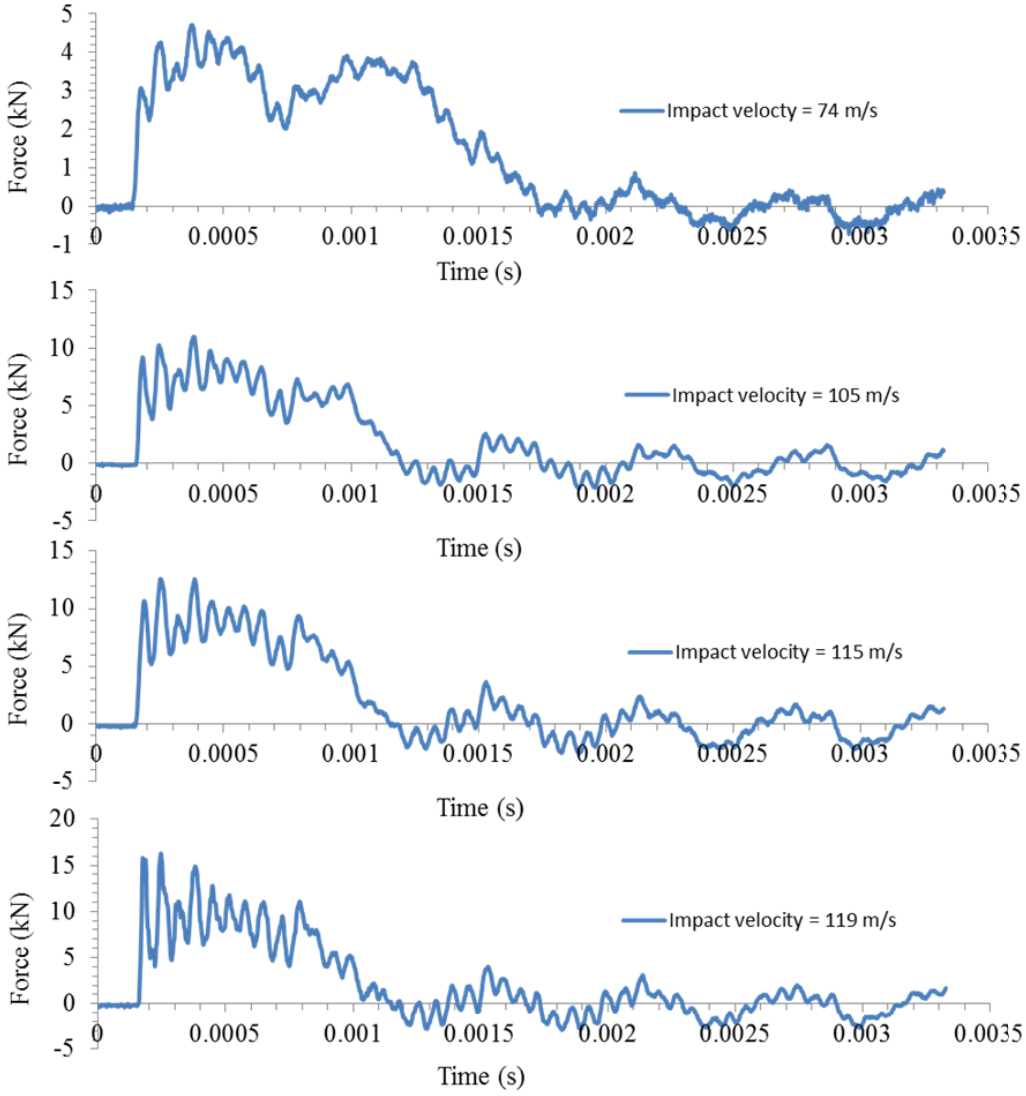

Figure 12: *Force-time history for the four impact velocities—74, 105, 115 and 119 m/s.*

4.3.1 Examining the oscillations observed in the force—time histories.

As in most time history data acquired in a test, the data could be converted from its original time domain to a frequency one using the Fourier Transform that is found in many data analysis package such as MATLAB [29], for example. Figure 13 shows the frequency domain for the four tests conducted and what could be observed are two identifiable frequencies, one at 2000 and the other at 15000 Hz that are present in all the results. Comparing the power amplitudes of these two frequencies, it is readily observed that they are influenced by the impact velocity and it may be necessary to remove these frequencies depending on their origins.

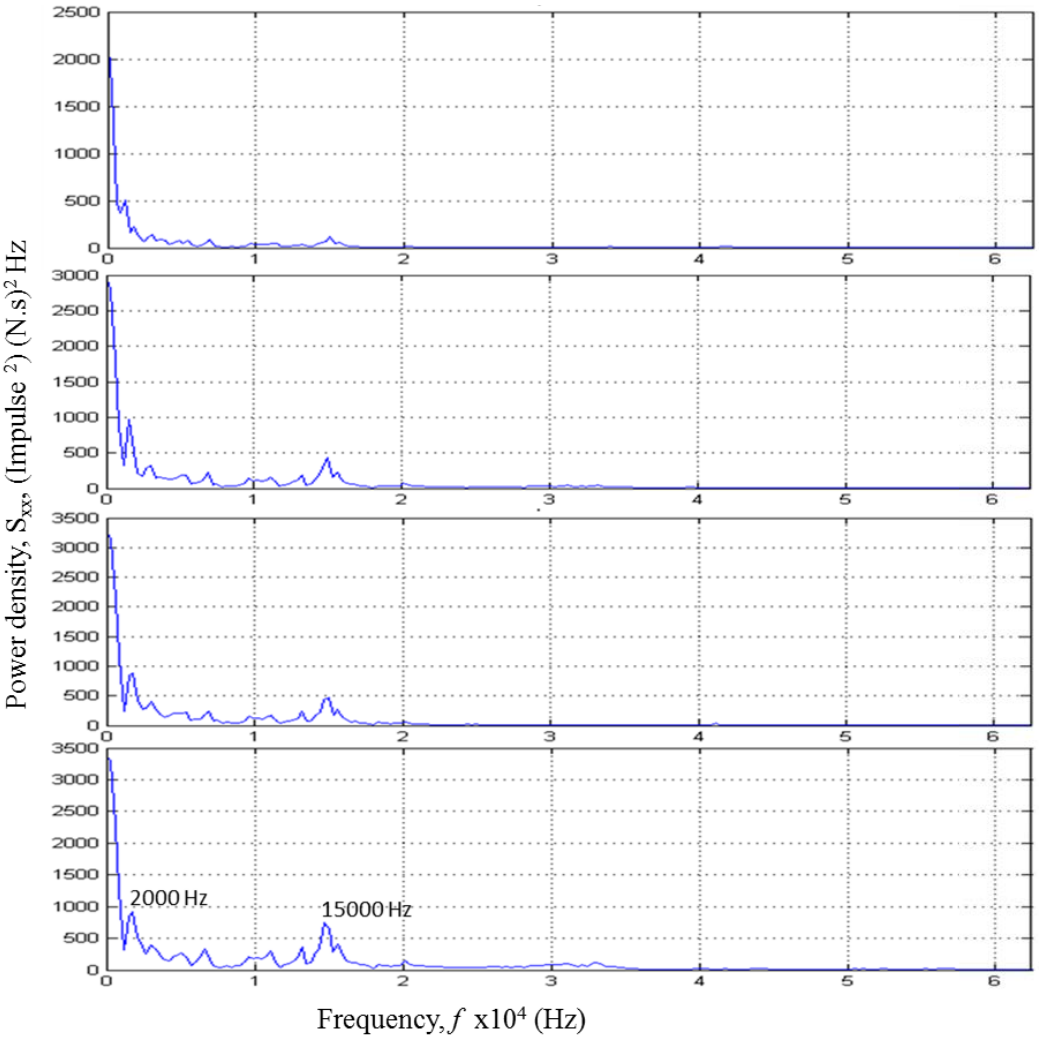

Figure 13: *The force-time curves in the frequency domain identifying frequencies that are present in the data.*

A manual roving hammer test was conducted, striking different parts of the target and its supporting structure. In the hammer tests conducted, the two frequencies were stimulated either when the target disc or supporting plate was struck. Neither frequency appeared when other parts of the surrounding structure was struck. Thus, these hammer tests simply indicated that these two frequencies were not generated by the projectile but came from the free vibrations of the target plate induced from the impact. Although the tests could not be used to identify which part of the target system, including the force ring transducer, the oscillations came from, there was a strong possibility that the frequencies came from the target disc and/or the supporting clamped plate that sandwiched the force ring transducer and, consequently, this needed to be verified.

4.3.2 Determination of the target disc and support plate frequencies using Bessel functions

The vibration and natural frequencies of plates is a subject that has long been studied extensively over many years by numerous researchers such as Lamb [30,31], Powell and Roberts [32], Southwell [33] and Robertson [34,35] to name a few. The 1977 work by Liessa [36,37] presents a comprehensive analysis of much of the literature available for the vibration of plates and presents an extensive and comprehensive set of available results for frequencies and mode shapes of free vibration of different types of plates for a wide variety of boundary an initial conditions. Liessa's [37] and the more recent study by Wu et al [38] are used in this study to determine the natural frequencies of the plates.

Obtaining the natural frequencies of plates depends very much on the boundary conditions thus, very slight misinterpretation of the boundary conditions could lead to erroneous results. As a result, understanding the equations is important and a brief description of the theory following that of Liessa [10] and Wu [11] is below but the reader is encouraged to consult these two references for more comprehensive details.

The transverse displacement, w of the elastic vibration of a plate could be determined using the classical wave equation

$$D\nabla^4 w + \rho\frac{\partial^2 w}{\partial t^2} = 0 \tag{17}$$

where $\nabla^4 = \nabla^2\nabla^2$ and $\nabla^2 = \frac{\partial^2}{\partial x^2} + \frac{\partial^2}{\partial y^2}$ is the Laplacian operator. D is the flexural rigidity defined as

$$D = \frac{Eh^3}{12(1-\nu^2)} \tag{18}$$

where ρ is the density, E is the Young's modulus, h is the plate thickness, and ν is the Poisson's ratio. When free vibrations are assumed the displacement in the wave equation can be expressed as

$$w = Wcos(\omega t) \tag{19}$$

where ω is angular frequency and W is amplitude as a function of position only. Substituting Equation (19) into (17) and separating the variables yield

$$\nabla^2 W_1 + k^2 W_1 = 0 \tag{20}$$

$$\nabla^2 W_2 + k^2 W_2 = 0 \tag{21}$$

where

$$k^4 = \frac{\rho\omega^2}{D} \tag{22}$$

Equations (20) and (21) are two linear differential equations whose solutions when superimposed provides a solution to Equation (17). To determine the component frequencies that are present in the free vibration of the plates, the Fourier transformation is used and is given by

$$W(r,\theta) = \sum_{n=1}^{\infty} W_n(r)\cos(n\theta) + \sum_{n=1}^{\infty} W_n(r)\sin(n\theta) \tag{23}$$

Substituting Equation (23) into Equations (20) and (21) transformed in polar coordinates gives the following differential equations

$$\frac{d^2 W_{n_1}}{dr^2} + \frac{dW_{n_1}}{dr} - \left(\frac{n^2}{r^2} - k^2\right) W_{n_1} = 0 \tag{24}$$

$$\frac{d^2 W_{n_2}}{dr^2} + \frac{dW_{n_2}}{dr} - \left(\frac{n^2}{r^2} - k^2\right) W_{n_2} = 0 \tag{25}$$

$$\frac{d^2 W^*_{n_1}}{dr^2} + \frac{dW^*_{n_1}}{dr} - \left(\frac{n^2}{r^2} - k^2\right) W^*_{n_1} = 0 \tag{26}$$

$$\frac{d^2 W^*_{n_2}}{dr^2} + \frac{dW^*_{n_2}}{dr} - \left(\frac{n^2}{r^2} - k^2\right) W^*_{n_2} = 0 \tag{27}$$

Equations (24) to (27) are recognized as forms of Bessel's equations having solutions of the form

$$W_{n_1} = A_n J_n(kr) + B_n Y_n(kr) \tag{28}$$

$$W_{n_2} = C_n I_n(kr) + D_n K_n(kr) \tag{29}$$

$$W^*_{n_1} = A^*_n J_n(kr) + B^*_n Y_n(kr) \tag{30}$$

$$W^*_{n_2} = C^*_n I_n(kr) + D^*_n K_n(kr) \tag{31}$$

where J_n and Y_n are Bessel functions of the first and second kinds, respectively, and I_n and K_n are modified Bessel function of the first and second kinds, respectively. The coefficients A_n, B_n, C_n and D_n determine the mode shape and are solved for using the boundary conditions. Thus, using Equations (28) to (31) a generalized solution to Equations (20) and (21) could be written as

$$\begin{aligned} W_n(r,\theta) = &\sum_{n=0}^{\infty} [A_n J_n(kr) + B_n Y_n(kr) + C_n I_n(kr) + D_n K_n(kr)] cos(n\theta) + \\ &\sum_{n=1}^{\infty} [A^*_n J_n(kr) + B^*_n Y_n(kr) + C^*_n I_n(kr) + D^*_n K_n(kr)] sin(n\theta) \end{aligned} \tag{32}$$

When the center of a polar coordinate system is taken to coincide with the with the center of the circular plate and the boundary conditions possess symmetry with respect to the diameter of the circular plate then the *sin* terms in Equation (32) are not needed. Setting

$$\lambda = (kr) \tag{33}$$

where k is given by Equation (22), for the n^{th} mode, Equation (32) is reduced to

$$W_n(r,\theta) = [A_n J_n(\lambda) + B_n Y_n(\lambda) + C_n I_n(\lambda) + D_n K_n(\lambda)]cos(n\theta) \tag{34}$$

For determining the free vibration frequency of the target disc, consider the photograph of the target system shown in Figure 9. The 120–mm disc that the projectile strikes is free to vibrate around the circumference and is fixed or supported at the center by a 28-mm cylindrical rod. In this case because the disc is fixed at the center over a 28-mm diameter area, it behaves very similar to an annular disc with a clamped 28-mm diameter hole at the center as was also observed by Aarønes [39] experimentally studying the natural frequencies of a disk. This implies that the boundary conditions for the annular disc are such that

$$W(b) = \frac{dW(b)}{dr} = 0 \tag{35}$$

$$M_r(a) = V_r(a) = 0 \tag{36}$$

where b in Equation (35) is the inner radius of the annulus. $M_r(a)$ is the bending moment and $V_r(a)$ is the reaction force which is zero at a, the outer radius of the annulus. Substituting Equation (34) into the boundary conditions given by Equations (35) and (36) for the first mode, $n = 0$, yields four homogeneous equations in A_n, B_n, C_n and D_n for which a non-trivial solution can exist only if the determinant of the coefficients is zero. Setting $\alpha = \frac{b}{a}$, Liessa [37] determined the frequency determinant in terms of the Bessel functions for the $n = 0$ mode and it is given by

$$\begin{vmatrix} J_0(\lambda) & Y_0(\lambda) & -I_0(\lambda) + \frac{2(1-\nu)}{\lambda} I_1(\lambda) & -K_0(\lambda) - \frac{2(1-\nu)}{\lambda} K_1(\lambda) \\ J_1(\lambda) & Y_1(\lambda) & I_1(\lambda) & -K_1(\lambda) \\ J_0(\alpha\lambda) & Y_0(\alpha\lambda) & I_0(\alpha\lambda) & K_0(\alpha\lambda) \\ J_1(\alpha\lambda) & Y_1(\alpha\lambda) & I_1(\alpha\lambda) & K_1(\alpha\lambda) \end{vmatrix} = 0$$

Table 3, taken from Liessa [37], presents, for a steel plate, the eigenvalues λ^2 obtained from the determinant by evaluating the Bessel functions for different $\alpha = \frac{b}{a}$ ratios.

Given that from Equation (33) $\lambda^2 = k^2 r^2 = k^2 a^2$ at $r = a$, substituting for k using Equation (22), λ^2 could be written as

$$\lambda^2 = \omega^2 r^2 \sqrt{\frac{\rho h}{D}} \tag{37}$$

Knowing that the angular frequency $\omega = 2\pi f$, where f is the frequency in Hz, Equation (37) could be rewritten as

$$f = \frac{1}{2\pi} \frac{\lambda^2}{a} \sqrt{\frac{D}{\rho h}} \tag{38}$$

Table 3: *Values of* $\lambda^2 = \omega a^2 \sqrt{\frac{\rho h}{D}}$ *for a free, clamped annulus, Liessa [10].*

$n=0$		$n=1$		$n=2$		$n=3$	
b/a	λ^2	b/a	λ^2	b/a	λ^2	b/a	λ^2
0.276	6.25	0.060	2.82	0.186	6.25	0.43	16
0.542	25.00	0.397	9.00	0.349	9.00	0.59	25
0.840	81.00	0.603	21.2	0.522	16.0	0.71	49

For the steel target disk used, the thickness is $h = 19\ mm$, the inner radius of the annulus is $b = 14.3\ mm$ and the outer radius is $a = 60\ mm$. Thus, using Table 3, a $b/a = 0.238$ ratio gives a $\lambda^2 = 6.25$ for the $n = 0$ mode. Taking the elastic modulus for steel as $E = 200\ GPa$, the Poisson's ratio as $\nu = 0.33$ and the density as $\rho = 7850\ kg/m^3$, using Equation (38) a frequency of $f_{disk} = 2000\ Hz$ is calculated. This is exactly one of the frequencies observed in Figure 13.

For rectangular plates, Wu et al [38] developed a similar Bessel function solution for the wave equation and in Cartesian coordinates it is given by

$$\begin{aligned} W_n(x,y) = &\sum_{m=-\infty}^{\infty} \left[A_n J_{m-n}(kx) J_m(ky) + B_n I_{n-m}(kx) + I_m(ky)\right] cos\left(\frac{m\pi}{2}\right) + \\ &\sum_{m=-\infty}^{\infty} \left[A_n J_{m-n}(kx) J_m(ky) + B_n I_{n-m}(kx) + I_m(ky)\right] sin\left(\frac{m\pi}{2}\right) \end{aligned} \tag{39}$$

For a clamped rectangular plate with sides a and b, the boundary conditions are such that

$$W(x=0) = W(x=a) = 0 \quad \frac{dW(x=0)}{dx} = \frac{dW(x=a)}{dx} = 0 \tag{40}$$

$$W(y=0) = W(y=b) = 0 \quad \frac{dW(y=0)}{dy} = \frac{dW(y=b)}{dy} = 0 \tag{41}$$

Using Equation (39) in the boundary conditions defined by Equations (40) and (41), Wu et al [38] constructed the vibration mode function

$$\begin{aligned} W_{n,m} = &\left(A_n \left\{J_{n-m}(kx) + J_{n-m}\left[k(a-x)\right]\right\} \left\{J_m(ky) + J_m\left[k(b-y)\right]\right\} + \right. \\ &B_n \left\{I_{n-m}(kx) + I_{n-m}\left[k(a-x)\right]\right\} \\ &\left. \left\{I_m(ky) + I_m\left[k(b-y)\right]\right\}\right) \cos\frac{m\pi}{2} \cos\frac{n\pi}{2} \end{aligned} \tag{42}$$

and showed that for a square plate, where $a = b$, with the boundary conditions described by Equations (40) and (41), Equation (42) can be satisfied with $m = \frac{n}{2}$, for $m \neq 0$. Setting $\lambda = ka$, the non-dimensional frequency and for a square plate $b = a$, the frequency determinant in terms of the Bessel functions that Wu et al [38] developed is given by

$$\det \begin{vmatrix} J_{n-m}(\lambda) & I_{n-m}(\lambda) \\ J'_m(\lambda) & I'_m(\lambda) \end{vmatrix} = 0$$

where $J_m^{'}(0)$ and $I_m^{'}(\lambda)$ the derivative of the Bessel function of the first kind. Wu et al [38] solved the determinant for the first 6 modes as a function of the non-dimensional frequency parameter λ and these are given in Table 4 below. Liessa [37] also found the non-dimensional frequency parameter for the same 6 modes using the Rayleigh-Ritz method and these are also given in Table 4. The values by Liessa [37], Wu et al [38] and from finite elements method [38] all compare very well.

Table 4: *First 6 sets of non-dimensional frequency parameter,* $\lambda^2 = \omega a^2 \sqrt{\frac{\rho h}{D}}$ *for a clamped square plate taken from Wu et al [38] and Liessa [37].*

Mode	λ^2, Wu et al [38]	λ^2, Liessa [37]	λ^2, Finite Element [38]
1	34.877	35.990	35.450
2	69.666	73.411	72.029
3	84.583	108.270	103.700
4	114.212	131.639	129.411
5	140.107	132.250	130.279
6	153.815	165.151	-

For the clamped square steel plate problem at hand, $a = 330\ mm$ and the thickness $h = 35\ mm$. Using the density, $\rho = 7800\ kg/m^3$, the elastic modulus $E = 200\ GPa$ and Poisson's ratio $\nu = 0.3$, the flexural rigidity, D, is calculated using Equation (18). From Table 4 taking $\lambda^2 = 36$ for the first mode and substituting for all the values in Equation (38) a frequency, $f_{plate} = 15000\ Hz$ is obtained. This is exactly the second frequency obtained from the Fourier transform of the force-time histories shown in Figure 13.

Knowing now that these two free vibration frequencies are influencing the force histories, they need to be removed and this is done in the next section.

4.3.3 Filtering of the unwanted oscillations

For the low frequency removal, a basic Butterworth band stop filter in MATLAB [29] was used. The resulting filtered signal obtained was not distorted and the low frequency of 2000 Hz was removed. However, using a band stop filter for the high frequency of 15000 Hz cause severe distortion and shifting of the resulting filtered curve. A literature review on high frequency filtering revealed that the Savitsky-Golay [40] filter was used with success in many domains for removing high frequencies and it was decided to use this for the problem at hand.

The Saviztky-Golay [40] filter is based on the least squares polynomial fitting across a moving window within the data in the time domain. As described by Acharya et al [41], the basic principle of the Savitsky-Golay [40] filter is to obtained $(2n + 1)$ equidistant points centered about $n = 0$ to represent a polynomial of degree p. The Savitsky-Golay

[40] filter computes the value of the least square polynomial over the entire sample space of $(2n+1)$ points. Typically, a long polynomial, or a moderate order one allows a high level of smoothing without attenuation of data features. As it turns out, the Saviztky-Golay [40] filtering method is better than averaging because it tends to preserve features of the data such as peak height and width, which are usually attenuated by the moving average filter. Furthermore, the symmetric Saviztky-Golay [40,41] filters have zero phase so that features of the signal are not shifted. Thus, if the signal has most of its energy in the passband of the filter (implying significant over-sampling), the signal components are undistorted while the high-frequency noise is reduced but not completely eliminated. In this fashion, the number of data samples, $(2n+1)$, of a particular frequency to be removed becomes important in determining the filter averaging window. For the filtering conducted on the force time histories in this study, n is chosen to be the number of sample points in one period of the oscillation to be removed.

The Savitsky-Golay [40] filter implemented in MATLAB [29] was used to conduct the filtering. Figures 14 to 18 show Force-Time/Sample data point (SDP) histories for the four different impact velocities. The original or raw data acquired is shown using the solid line curve. In the 119 m/s impact velocity case, for the high frequency oscillations, the $2n$ data points, indicated by SDP in Figure 14, is $(193-123)=70$. Thus, the frame length for the averaging window for the high frequency is 71, $(2n+1)$. Table 5 shows the frame lengths chosen for removing the high frequencies for the four different impact velocity cases. In

Table 5: *The Savitsky-Golay [40,41] filter frame length for the high frequency removal for different impact velocities.*

Impact velocity (m/s)	High Frequency Frame length $(2n+1)$
119	71
115	71
105	71
74	61

Figures 14 to 17, the dashed and dotted curves show, respectively, the data with the high and low frequencies removed. Figures 18 to 21 show the final filtered data with the identification of force caused by the shock pressure. This is taken to be the maximum force arrived at after the steep rise and corresponds to essentially to highest peak identified in the raw data history in order to be consistent. The remainder of the force-time curve would indicate the steady state loading of the target by the projectile until it is completed eroded or it has rebounded. In the 74 m/s impact velocity case Figures 17 and 21 will show two peaks in the force-time curve. In this case the video showed that the projectile broke into two pieces before impact. Thus, essentially there were two impacts occurring onto the target. The impact velocity of the second part may have been be a little lower than 74 m/s given that it seemed to have struck the back end of the first part of the projectile before coming

into contact with the target. For this reason the results are slightly inconsistent with those of the other tests.

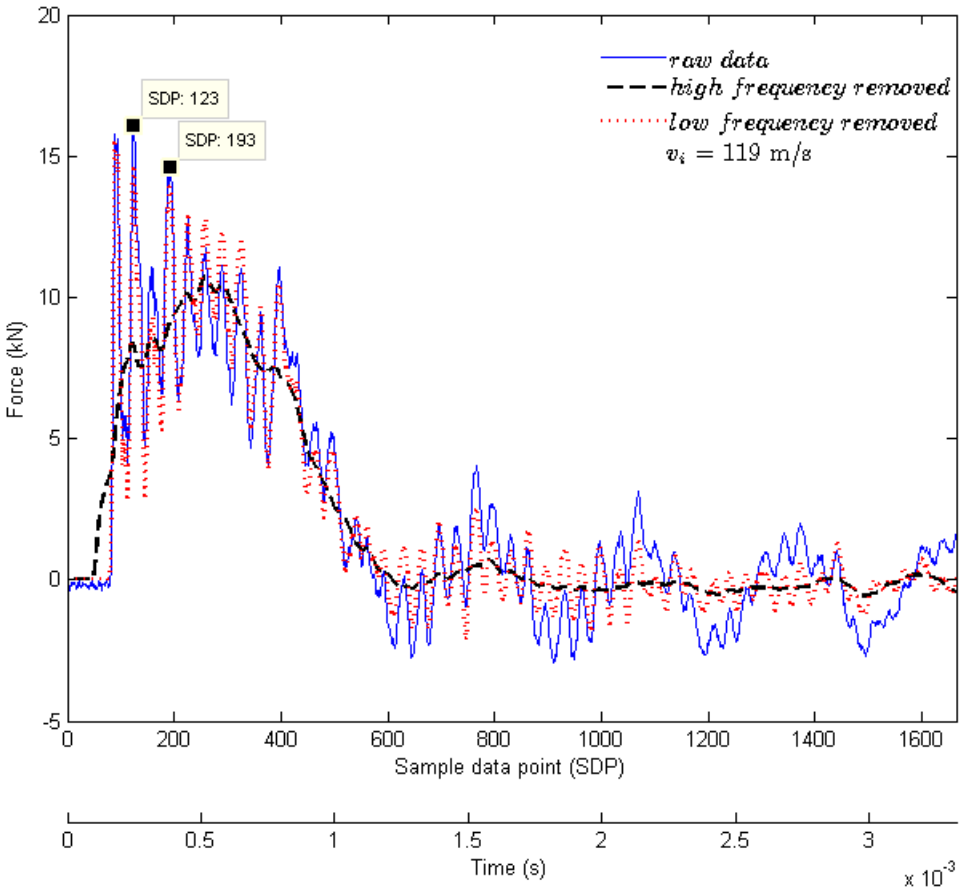

Figure 14: *Comparison of raw force-time curve with the filtered curve for the 119 m/s impact velocity case.*

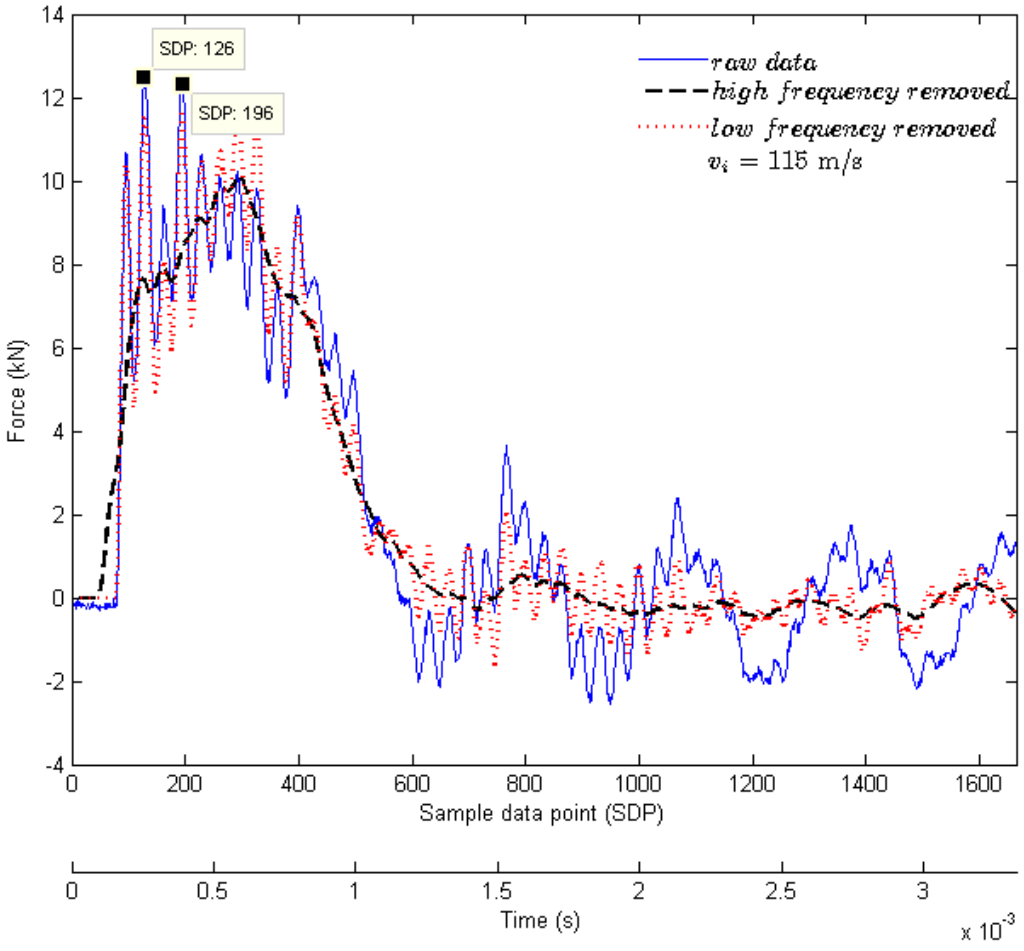

Figure 15: *Comparison of raw force-time curve with the filtered curve for the 115 m/s impact velocity case.*

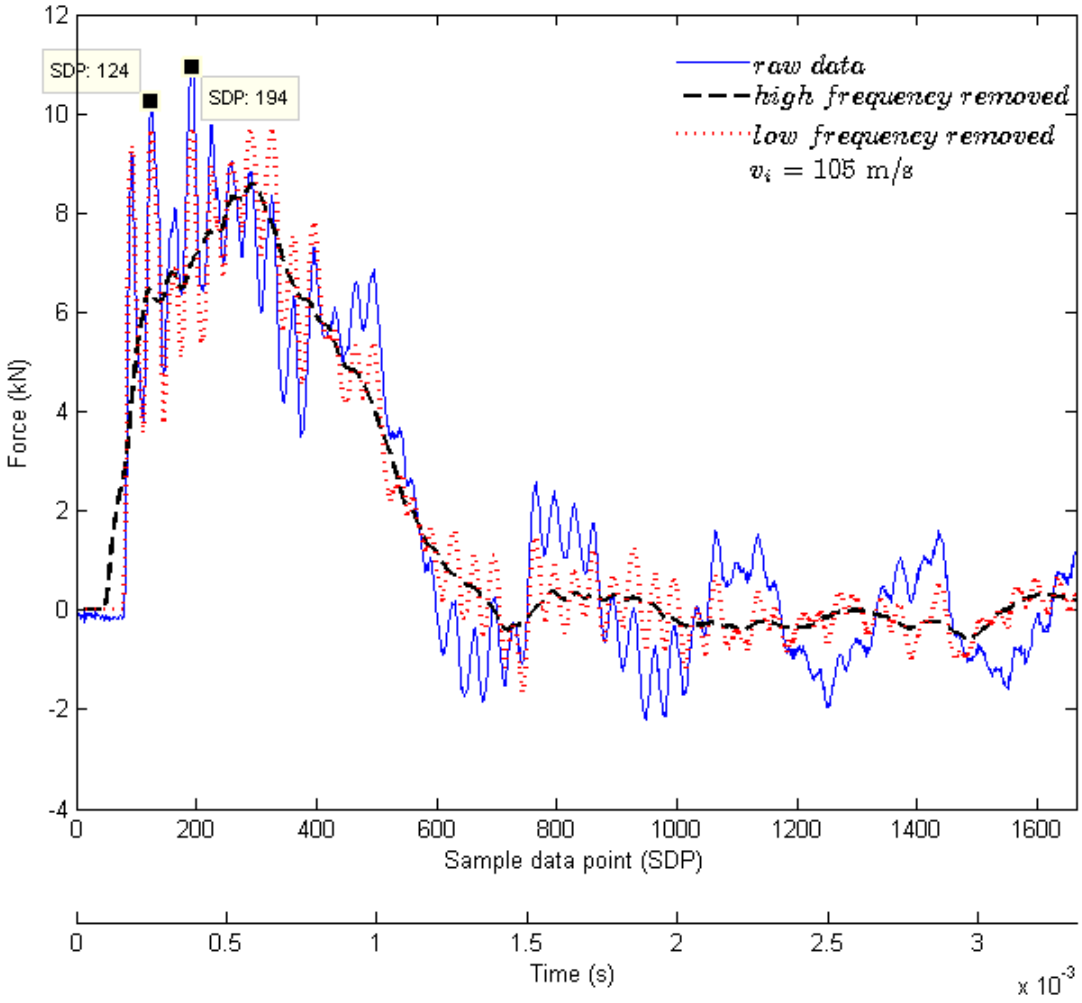

Figure 16: *Comparison of raw force-time curve with the filtered curve for the 105 m/s impact velocity case.*

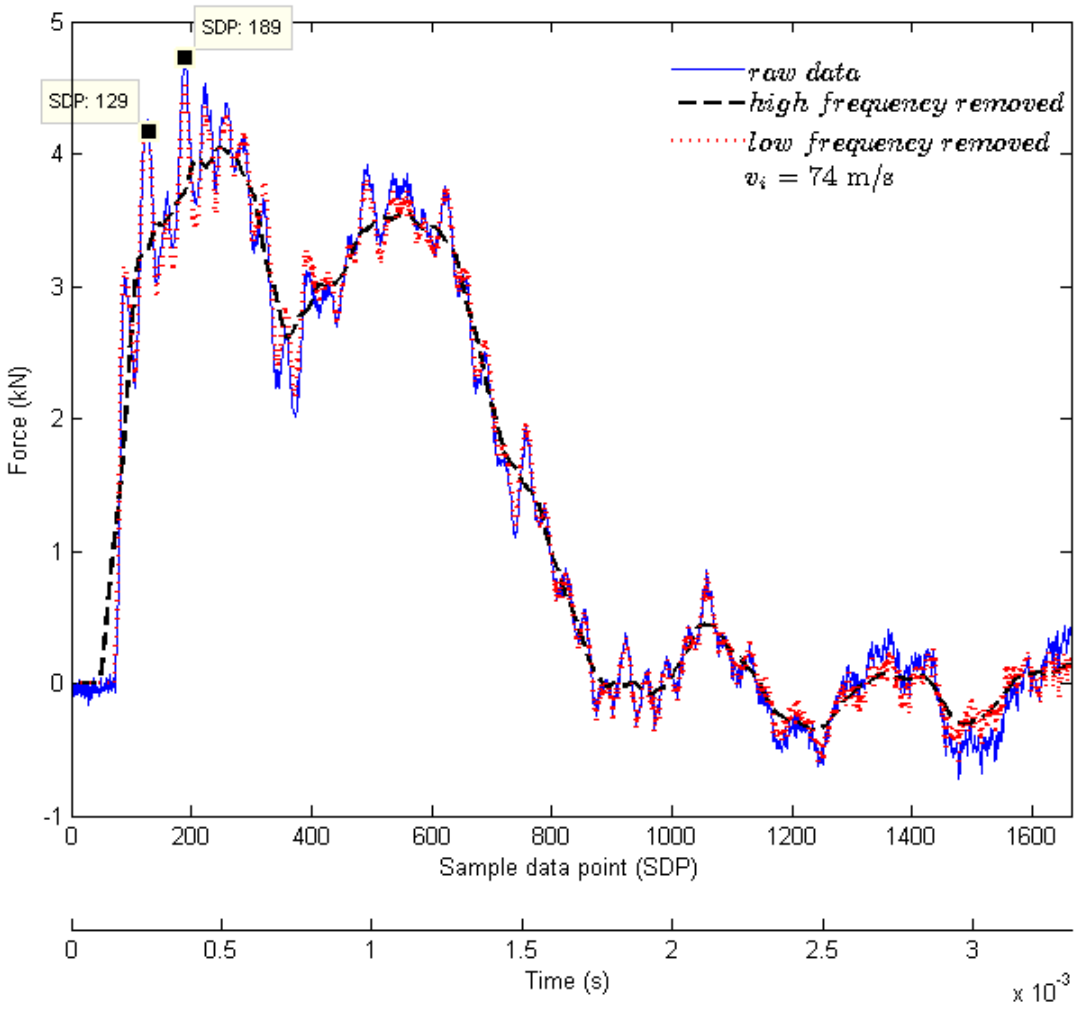

Figure 17: *Comparison of raw force-time curve with the filtered curve for the 74 m/s impact velocity case.*

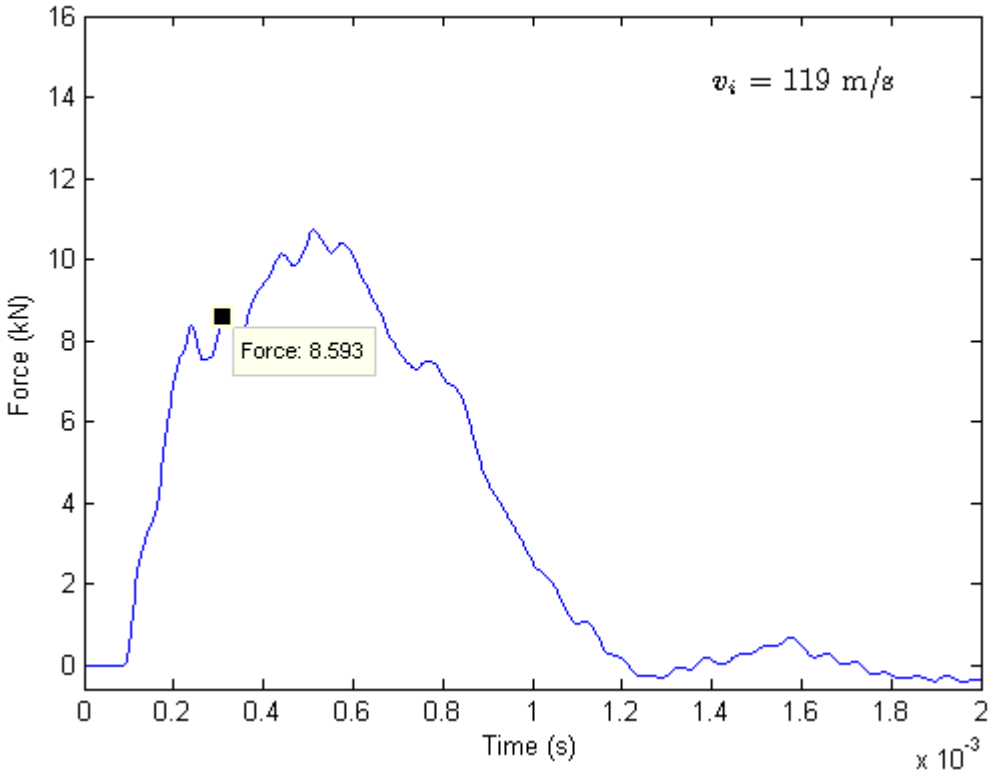

Figure 18: *The force-time curve indicating the shock force for the 119 m/s impact velocity case.*

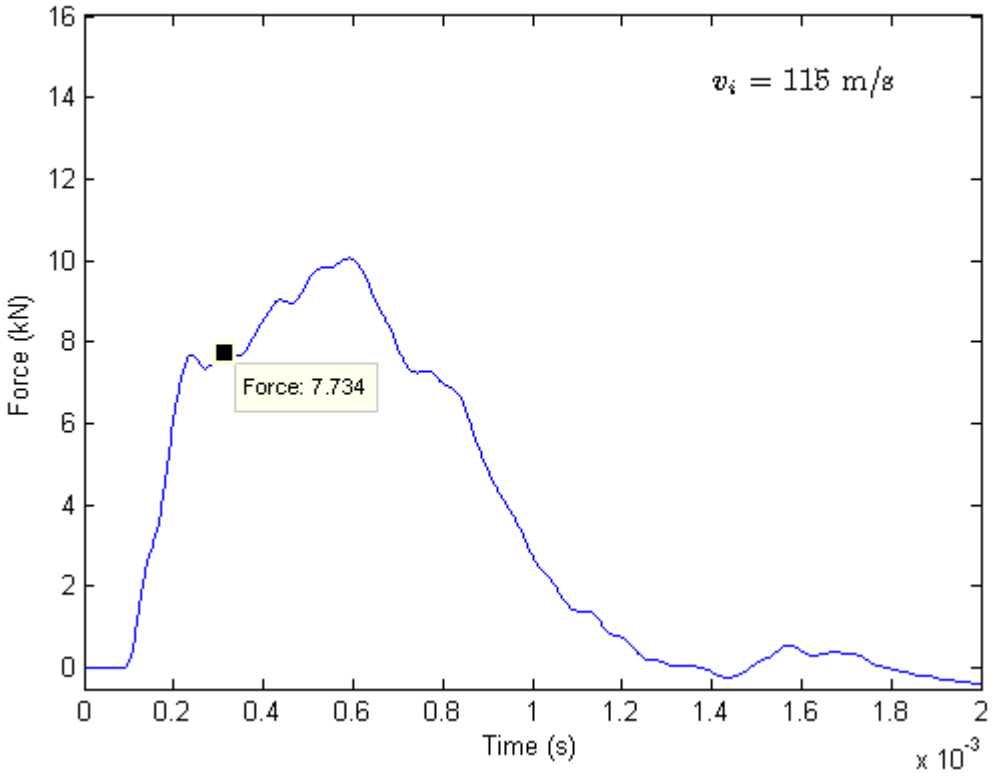

Figure 19: *The force-time curve indicating the shock force for the 115 m/s impact velocity case.*

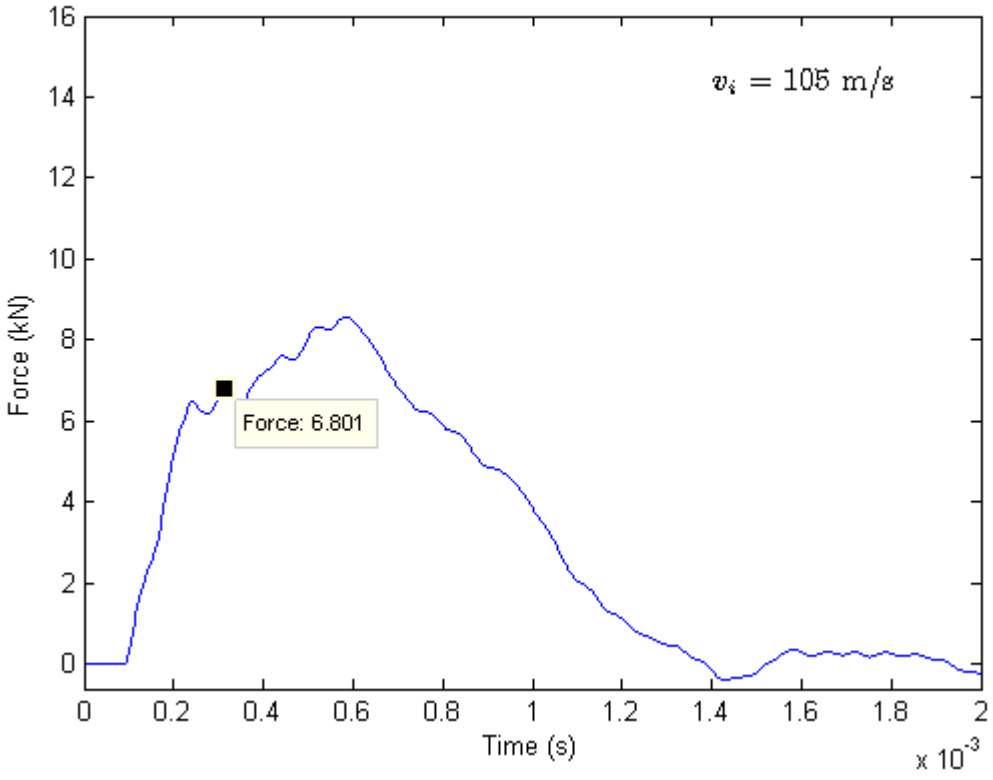

Figure 20: *The force-time curve indicating the shock force for the 105 m/s impact velocity case.*

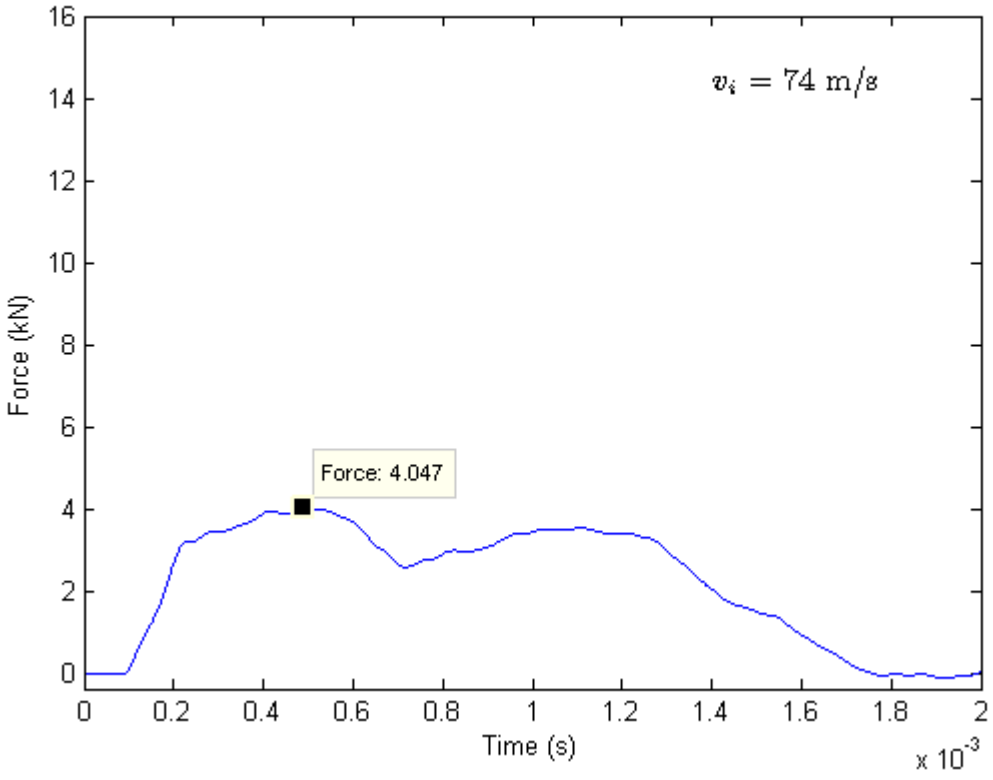

Figure 21: *The force-time curve indicating the shock force for the 74 m/s impact velocity case.*

From the filtered data shown in Figures 18 to 21 the maximum force at impact for each striking velocity was determined and are shown in Table 6 below along with the unfiltered maximum force. Figure 22 shows a plot of the raw data maximum force and that from the filtered data as a function of the impact velocity and it is obvious from the graph that as the impact velocity increases the free vibrational frequencies of the target and supporting plates significantly influence the measured force.

Table 6: *Comparison of measured maximum force with that obtained from filtered data as a function of impact velocity.*

Impact velocity (m/s)	Measured maximum force (kN)	Filtered maximum force (kN)
119	16.47	8.59
115	12.79	7.73
105	11.15	6.80
74	4.79	4.05

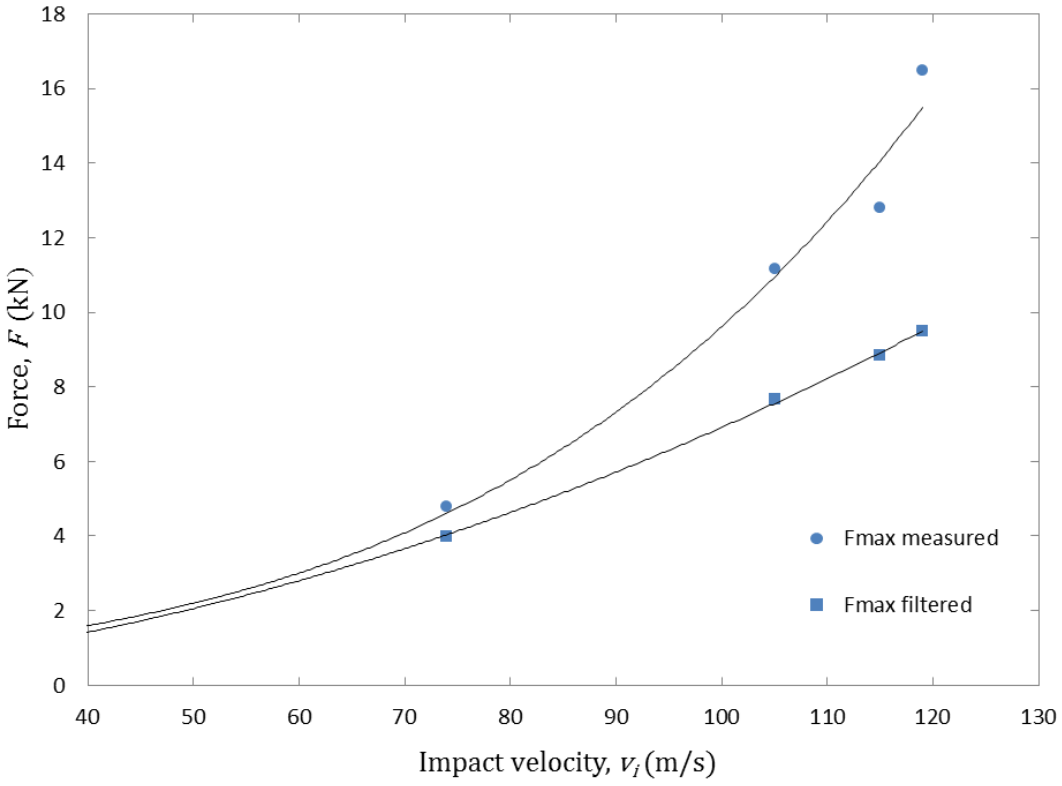

Figure 22: *Measured maximum force with and without filtering as a function of impact velocity.*

4.3.4 Examining the impedance mismatch on the shock pressure

When a wave travelling in a medium encounters another medium with a different density then part of the wave will continue to propagate into the new medium and part of the wave will be reflected back into the original medium. The part that propagates in the new medium is known as the transmitted wave whereas the part that propagates in the original medium is known as the reflected wave. The ease with which an ultrasonic pulse can travel through a material depends on a property called the impedance, Z. This is normally defined as the product of the material's density and its characteristic acoustic velocity. Thus,

$$Z = \rho c_0 \tag{43}$$

where ρ is the density and c_0 is the acoustic velocity. In the case of normal incidence, where the propagation direction of the shock is orthogonal to the target surface, the amplitude of the transmitted and reflected waves depend only on the change of impedance between the two media and this is referred to as the impedance mismatch.

For the problem at hand, on impact of the projectile onto the target, a shock pressure is generated at the interface between the projectile and the target but because of the impedance mismatch the pressure generated divides up into the transmitted pressure pulse that is transmitted into the target and the reflected pulse that is reflected back into the projectile. The force transducer attached to the back side of the target disc, responds to the transmitted pressure pulse and this shows up at the beginning of the force history signal and, thus, the maximum force measured here provides a measure of the transmitted shock pressure. Knowing the transmitted pressure could in turn be used to obtain the interface shock pressure. A material under shock loading would be considered to have a shock impedance where c_0 in Equation (43) would be replaced with the shock speed, U_s. This is very well described by Cooper [21]. Studies, for example Cleveland et al [42], have shown that the fraction of the impact shock pressure wave that is transmitted through the target is given by the transmission coefficient, T_t as

$$T_t = \frac{2Z_2}{Z_1 + Z_2} \tag{44}$$

whereas, for the reflected wave, the coefficient, T_r, is given by

$$T_r = \frac{Z_2 - Z_1}{Z_1 + Z_2} \tag{45}$$

where U_{s1} and U_{s2} are the shock speeds in medium 1 and 2, respectively. $Z_1 = \rho_1 U_{S1}$, $Z_2 = \rho_2 U_{S2}$ are the shock impedance for medium 1 and 2, respectively, and $T_t + T_r = 1$. Because of this condition, medium 2 would be assigned to the gelatine projectile which has the lower impedance of the two materials in contact whereas medium 1 would be assigned to the steel target. Thus, given that the force transducer is at the back of the target plate, the amplitude of the force measured at the beginning of force time history would be the transmission fraction, T_t, of the original shock pressure at the projectile/target interface.

Table 7 shows a summary of the important results for the four tests conducted. For each impact velocity, v_i, the corresponding interface particle velocity, u_p was calculated using Equation (7). This in turn was used to calculate the shock speeds in the steel target and the gelatine projectile, U_{steel} and $U_{gelatine}$ using Equation (1). The shock speeds were then used to calculate the material shock impedance which were used to evaluate the transmission and reflective coefficients T_t and T_r using Equations (44) and (45). Knowing the force, F_{max} the transmission coefficient is used to determine the interface shock pressure, P_h. For example, for the case where $v_i = 119$ m/s, $T_t = 0.073$, thus, 7.3% of the of the interface shock pressure was transmitted. Scaling this to 100% and dividing by the cross sectional area of the projectile, 0.000616 m^2, an interface pressure, P_h, of 191 MPa was obtained.

Table 7: *A summary of results giving the impact velocity, v_i, the interface particle velocity, u_p, shock speed in steel target and gelatine projectile, U_{steel} and $U_{gelatine}$, the transmission and reflective coefficients, T_t and T_r, the filtered experimental force measured, F_{max} and the interface pressure, P_h.*

v_i (m/s)	u_p (m/s)	U_{steel} (m/s)	$U_{gelatine}$ (m/s)	T_r	T_t	F_{exp} (kN)	P_h (MPa)	P_h (MPa)
119	3.8	5806	1663	0.927	0.073	8.59	191	196
115	3.8	5806	1655	0.927	0.073	7.73	174	189
105	3.8	5805	1637	0.923	0.072	6.80	154	171
74	2.7	5804	1581	0.931	0.069	4.05	95	116

Figure 23 shows a graph taken from Figure 4 for the theoretical interface pressure, P_h, as a function of impact velocity but with the calculated experimental pressure given in Table 6. It is immediately seen that the experimental results compares very well with the theoretical values.

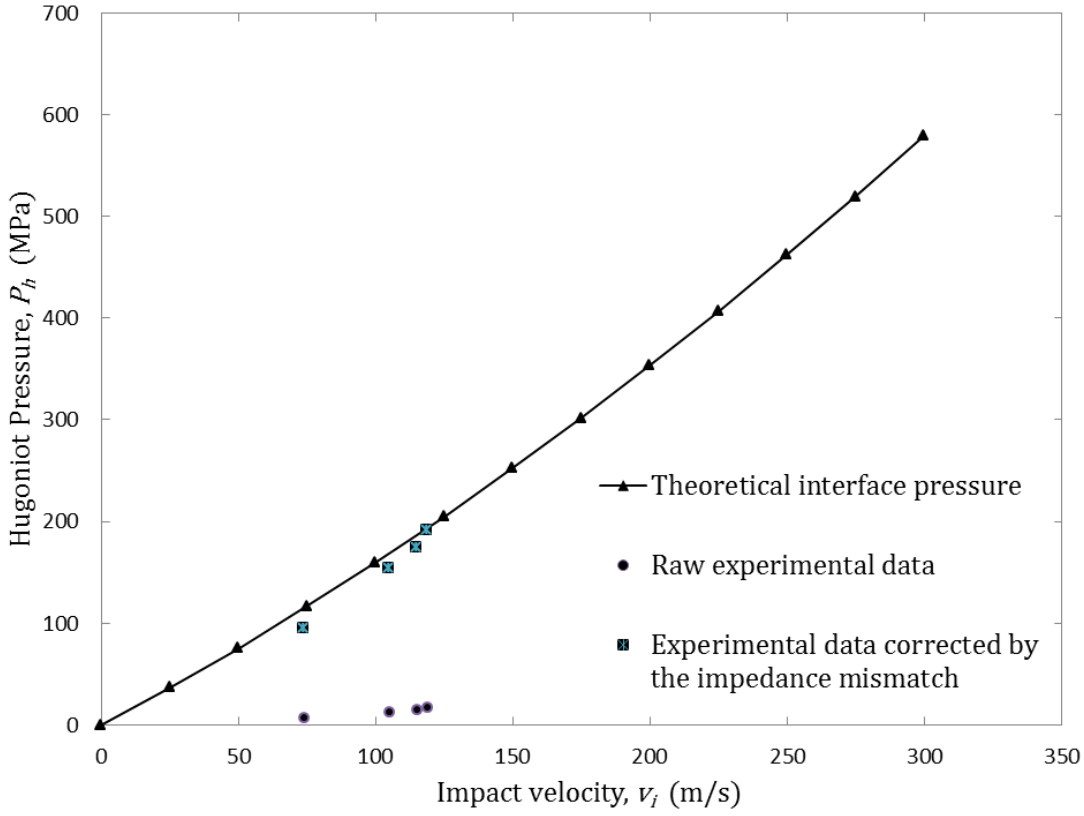

Figure 23: *Comparison of the calculated experimental shock pressure with the theoretical value as a function of impact velocity.*

4.3.5 Examining the experimental results for the steady state pressure

For the particular impact problem at hand where the penetration velocity is zero given that the target is rigid, it was shown earlier in Section 3 that the Alekseevski-Tate equations, Equations (9) to (13) lend themselves very well in determining the steady state impact conditions such as the projectile erosion rate, the time the projectile spends on the target and the steady state interface pressure applied.

Equation (14) shows that the rate of change of the projectile length or its erosion rate is simply the impact velocity. Performing the integration of Equation (14) gives Equation (15) which provides the time the projectile spends loading the target. The results shown in Table 8 shows that the time obtained analytically compares very well with the experimental values.

Table 8: *Comparison of experimentally measured time spent by the projectile with that obtained analytically from the Alekseevski-Tate equation.*

Impact velocity (m/s)	Projectile length (mm)	Measured time (ms)	Time from Alekseevskii-Tate Equation (15)(ms)
119	102.5	0.87	0.88
115	102.0	0.90	0.89
105	102.8	1.00	0.98
74	102.3	1.40	1.38

With respect to the steady state interface pressure, in accordance with Equation (10), if the strength of the projectile material, Y_p, is assumed to be negligible then Equation (10) reduces to the well-established [10,11,12] steady state stagnation pressure at the interface, $P_{stagnation} = \frac{1}{2}\rho v_i^2$. However, interpretation of the experimental results does not seem to indicate this. Consider the experimental results shown in Figures 24 to 27, $P_{stagnation}$ is plotted on the same axes as the experimentally derived pressure-time curves. Examination of the two curves reveals that the $P_{stagnation}$ is much lower than the experimentally derived pressure by an amount, ΔP. This indicates the presence of a dynamic pressure that the projectile material is applying to the target and is of the order of the shock pressure. This observation could be explained in accordance with Equation (10) $P_{interface} = \frac{1}{2}\rho_r v^2 + Y_p$. If Y_p is taken into consideration [28], then setting $Y_p = \Delta P$, Y_p could be termed as a dynamic pressure applied by the gelatine and it is impact velocity dependent. It would seem difficult to imagine that this could not be due alone to the strength of the projectile as is often used in the case of other solid penetrators materials, because studies [43,44] have shown that the fracture strength of gelatine at reasonably high strain rates is between 1–2 MPa so there must be other phenomena occurring. A close observation of the projectile/target interface provides one explanation. It appears that the gelatine material in the mushrooming region

of the projectile is undergoing severe compression enough to cause a significant increase in the bulk modulus which in turns manifests itself in a localised increase in the bulk density enough to cause a significant rise in the pressure applied to the target. This continues for about half way through the length of the projectile interaction with the target after which the interface pressure dropped linearly to zero as the projectile erodes away. Table 9 presents the quasi static and strain rate data from Cronin et al [43] and Winter et al [44] along with peak dynamic pressure obtained from this study. It would be worthwhile to note that the data from Winter et al [44] is for 20% gelatine which has s density of 1060 kg/m^3 comparing to the 10% gelatine that is used in this study and that of Cronin et al [43] that has a density of 1030 kg/m^3. This would seem to be a reasonable inclusion to make for guidance. Figure 28 shows ΔP as a function of impact velocity and a quadratic fit to the data indicates that the peak dynamic pressure at the interface rapidly increases with impact velocity.

Table 9: *Experimental dynamic pressure, ΔP, as determined in accordance with the Alekseevsii-Tate Equation (10).*

Impact velocity (m/s)	$P_{stagnation} = \frac{1}{2}\rho v_i^2$ (MPa)	Peak dynamic strength ΔP (MPa)
Cronin et al [41] (.01 s^{-1})	-	1
Winter et al [40] (Quasi static)	-	0.04
Winter et al [40] (920 s^{-1})	-	1.1
119	1.40	244
115	1.00	228
105	0.90	195
74	0.87	92

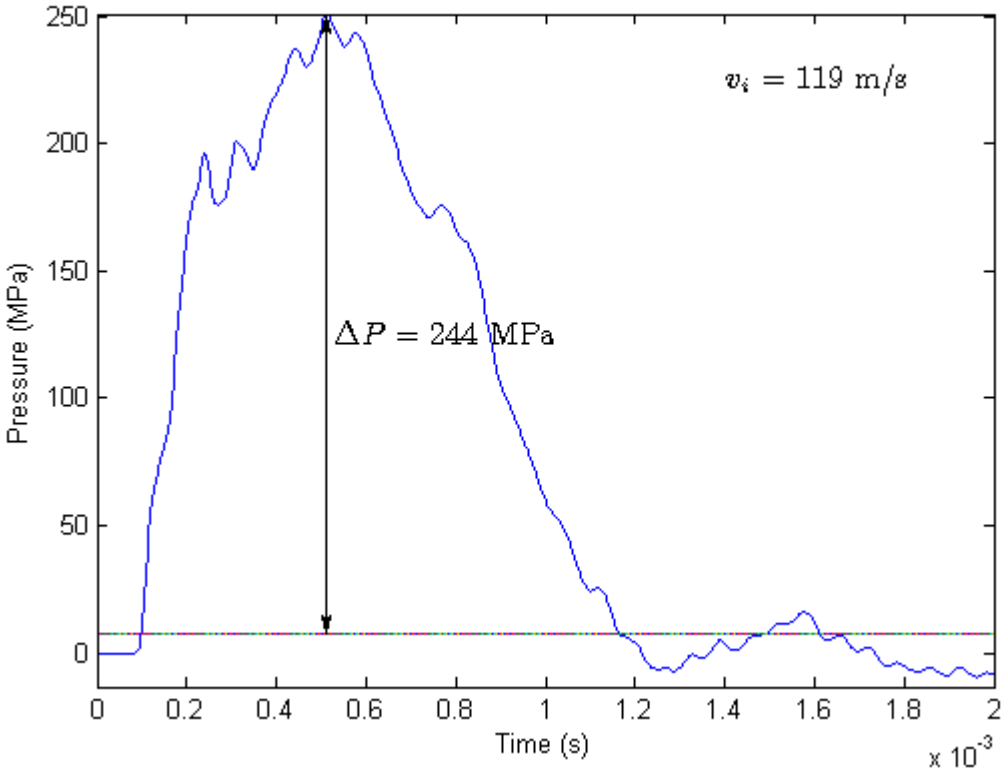

Figure 24: *Dynamic strength of the gelatine projectile, ΔP, for the 119 m/s impact velocity case.*

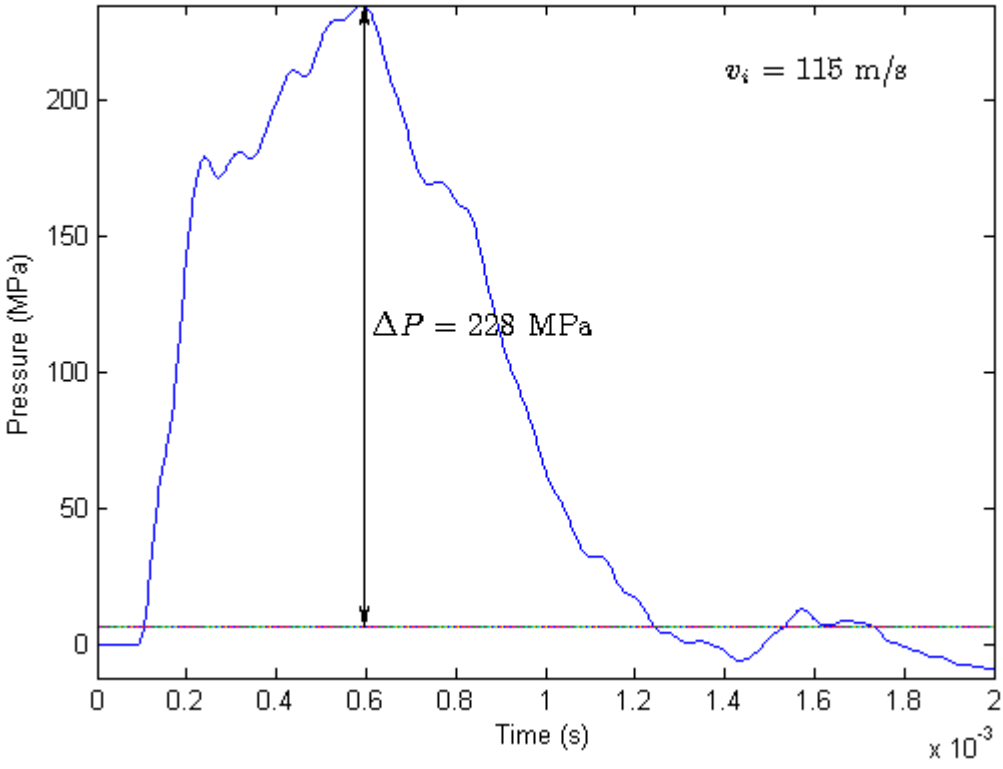

Figure 25: *Dynamic strength of the gelatine projectile, ΔP, for the 115 m/s impact velocity case.*

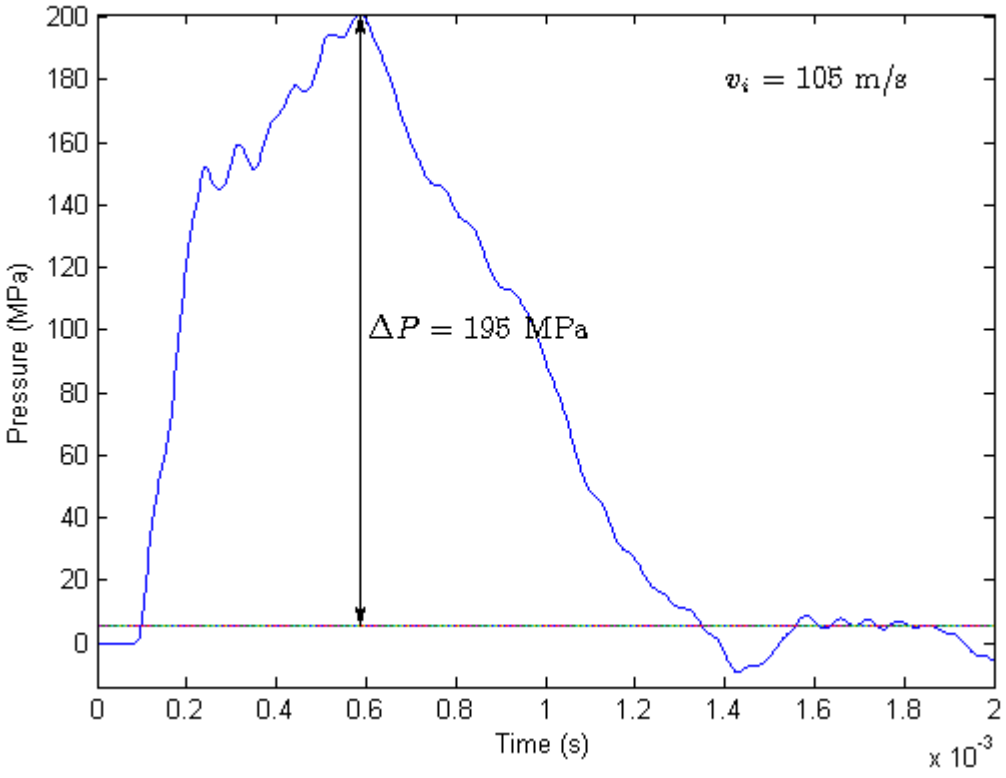

Figure 26: *Dynamic strength of the gelatine projectile, ΔP, for the 105 m/s impact velocity case.*

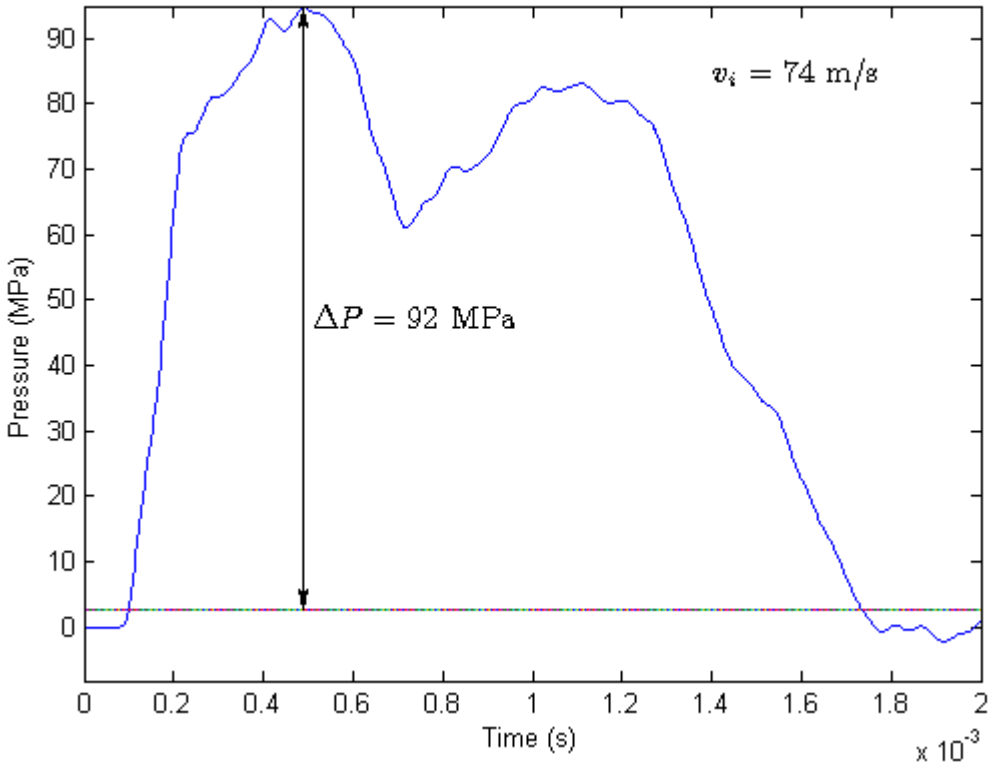

Figure 27: *Dynamic strength of the gelatine projectile, ΔP, for the 74 m/s impact velocity case.*

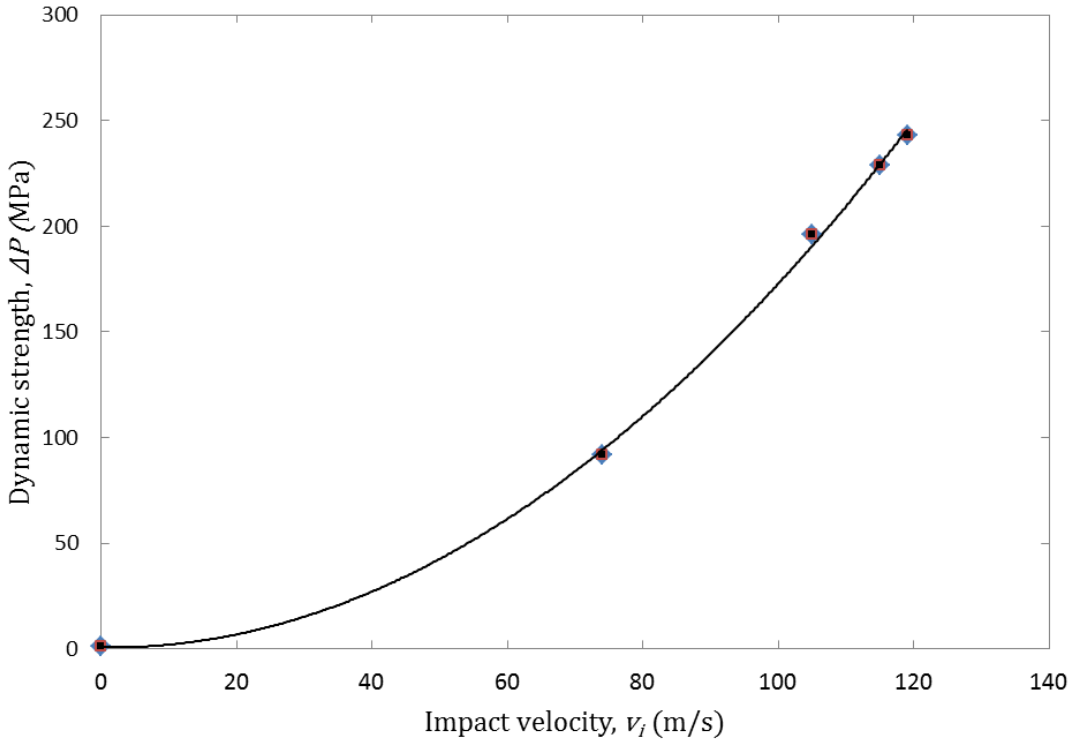

Figure 28: *Dynamic strength of the gelatine projectile as a function of impact velocity.*

5 Conclusion

The work presented in this report examines the impact process of a soft body material projectile, which in this case is made of 10% gelatine, striking a rigid target attached to a quartz force ring sensor. The basic objective was to examine a newer approach to determine whether the projectile/target interface parameters such as the shock and steady state pressures could be determined from the measured force-time history and to present validated experimental data that could be used for material constitutive model development for simulation of the impact or shock loading of soft body materials. Using the shock Hugoniot relations and the conservations equations, a theoretical shock pressure relation was obtained for the shock pressure imparted into the target and the projectile at the interface. The Alekseevskii-Tate penetration equations were used to determine the steady state pressure applied to the target.

Impact tests were conducted with 10% gelatine projectiles and the force-time histories were measured. The force time curves were examined to identify frequencies that were present in the results and may be coming from the natural vibrations of the various parts that make up the target. Vibration analysis methods such as the Bessel function solutions for the wave equation applied to the free vibration of plates were used to obtain the frequencies of the various plates in the target assembly. Once these frequencies were identified and determined that they did not form part of the loading, they were removed using the Savitsky-Golay filter. From the filtered Force-time histories, the shock pressures were derived and very good comparison was obtained when compared to the theoretical values predicted by the shock Hugoniot.

The Alekseevskii-Tate penetration equations were used to determine the steady state pressure at the projectile/target interface and the duration of the interaction between the projectile and target. The equations predicted very well the duration of the interaction. However, the measured value of the steady state pressure was in discordance with the expected stagnation pressure, $P_{stagnation} = \frac{1}{2}\rho v_i^2$. The presence of a dynamic pressure was observed and when interpreted in accordance with the Alexseevskii-Tate equation, suggests that the material dynamic strength manifested from the compression of the gelatine material caused a change in the bulk modulus or density and, thus, resulting in an increased pressure. A quantitative measure of this dynamic strength as a function of time was obtained and it is dependent on the impact velocity. Given the significant value of this dynamic pressure, it may be necessary to take this into account when these materials are used in shock loading and impact scenarios.

References

[1] Wilbeck, J.S., Impact Behavior of Low Strength Projectiles, Technical Report AFML-TR-71(2), Wright-Patterson Air Force Base, Dayton, OH, 1978.

[2] Heimbs, S., Computational Methods for Bird Strike Simulations: A Review, *Comput Struct*, 89 (23–24), pp. 2093–2112, 2011.

[3] Hedayadti, R. and Sadighi, M., Bird Strike, An Experimental, Theoretical and Numerical Investigation, *Woodhead Publishing in Mechanical Engineering*, Elsevier, Cambridge, UK, 2016.

[4] Barber J.P., Taylor, H.R. and Wilbeck, J.S., Characterization of Bird Impacts on a Rigid Plate: Part 1, Technical Report AFFDL-TR-75-5, Air Force Flight Dynamics Laboratory, OH, 1975.

[5] Barber J.P., Taylor, H.R. and Wilbeck, J.S., Bird Impact Forces and Pressures on Rigid and Compliant Targets. Technical Report AFFDL-TR-77-60, Air Force Flight Dynamics Laboratory, OH, 1978.

[6] Wilbeck, J.S. and Barber, J.P., Bird Impact Loading, *Shock Vibration Bulletin*, Vol. 48, i2, pp. 115–122, 1978.

[7] Lavoie, M.A., Gakwaya, A., Nejad Ensan, M. and Zimcik, D.G., Validation of available approaches for numerical bird strike modeling tools, *International Review of Mechanical Engineering*, v1 (4), pp. 380–389, 2007.

[8] Lavoie, M.A., Gakwaya, A., Nejad Ensan, M., Zimcik, D.G. and Nandlall, D., Bird Substitutes Tests Results and Evaluation of Available Numerical Methods, *International Journal of Impact Engineering*, 36(10), pp. 1276–1287, 2009.

[9] Liu, G., Li, Y. and Gao, X., Bird Strike on a Flat Plate, Experiments and Numerical Simulations, *International Journal of Impact Engineering*, 70, pp. 21–37, 2014.

[10] Hopkins, H.G. and Kolsky, H., Mechanics of Hypervelocity Impact of Solids, *Proceedings of the Fourth Symposium on Hypervelocty Impact*, Paper No. 12, Air Force Proving Ground Center, Eglin Air Force Base, Florida, 1960.

[11] Hopkinson, B., A Method of Measuring the Pressure Produced in the Detonation of High Explosive or by the Impact of Bullets, *Philosophical Transactions of the Royal Society of London, A*, Vol. 213, pp. 437–466, 1914.

[12] Birchoff, G., MacDougall, D.P., Pugh, E.M., and Taylor, G.I., Explosives with Lines Cavities, *Journal of Applied Physics*, Vol. 19, No. 6, pp. 563–582, 1948.

[13] Heymann, F.J., On the Shock Wave Velocity and Impact Pressure in High-Speed Liquid-Solid Impact, *Transactions of the ASME, Series D, Journal of Basic Engineering*, Vol. 90, pp. 400–402, 1968.

[14] Johnson, W. and Vickers, G.W., Transient Stress Distribution Caused by Water Jet Impact, *Journal of Mechanical Engineering Science*, Vol. 15, No. 4, 1973.

[15] Bowden, F.P. and Brunton, J.H., The Deformation of Solids by Liquid Impact at Supersonic Speeds, *Proceedings of the Royal Society, London, Series A*, Vol. 263, pp. 433–450, 1961.

[16] Brunton, J.H., The Physics of Impact and Deformation: Single Impact, *Philosophical Transactions of the Royal Society of London, A*, Vol. 260, pp. 73–85, 1966.

[17] Bowden, F.P. and Field, J.E., The Brittle Fracture of Solids by Liquid Impact, by Solid Impact and by Shock, *Proceedings of the Royal Society of London, Series A*, Vol. 263, pp. 331–352, 1964.

[18] Glenn, L.A., On the Dynamics of Hypervelocity Liquid Jet Impact on a Flat Rigid Surface, J*ournal of Applied Mathematics and Physics, (ZAMP)*, Vol. 25, pp. 383–398, 1974.

[19] Cook, S.S., Erosion by Water-Hammer, *Proceedings of the Royal Society of London, Series A*, Vol. 119, pp. 481–48, 1928.

[20] Gojani, A.B., Ohtani, K., Takayama, K. and Hosseini, S.H.R., Shock Hugoniot and Equations of States of Water, Castor Oil and Aqueous Solutions of Sodium Chloride, Sucrose and Gelatin, *Shock Waves*, Vol. 26, Issue 1, pp. 63–68, 2016.

[21] Cooper, P.W., Explosives Engineering, VCH, New York, 1996.

[22] Carlucci, D.E. and Jacobson, S.S., Ballistics: Theory and Design of Guns and Ammunition, *CRC Press*, Taylor and Francis Group, LLC, Boca Raton, FL, 2008.

[23] Alekseevskii, P., Penetration of a Rod Into a Target at High Velocity, *Combustion Explosion and Shock Waves*, Vol. 2, pp. 63–66, 1966.

[24] Tate, A., A Theory for the Deceleration of Long Rods after Impact. *J. Mech. Phys. Solids*, vol. 15, pp. 387–399, 1967.

[25] Walters, W.P. and Segletes, S.B., An Exact Solution of the Long Rod Penetration Equations, *International Journal of Impact Engineering*, Vol. 11, no. 2, pp. 225–231, 1991.

[26] Segletes, S.B. and Walters, W.P., Efficient Solution of the Long-Rod Penetration Equations of Alekseevskii-Tate, ARL Report ARL-TR-2855, US Army Research Directorate, AMSRL-WM-TD, Aberdeen Proving ground, MD, 2002.

[27] Walters, W.P. and Williams, C., A Solution of the Alekseevskii-Tate Equations, ARL Report ARL-TR-3606, US Army Research Directorate, AMSRL-WM-TD, Aberdeen Proving ground, MD, 2005.

[28] Flis, W.J., Modified Alekseevskii-Tate Model for Rod Penetration of Porous Targets, *Proceedings of the* 28^{th} *International Symposium on Ballistics*, Edinburgh, Scotland, UK, pp. 2219–2227, 2016.

[29] MATLAB, version R2013b (8.20.701), The MathWorks Inc., Natick, MA, 2013.

[30] Lamb, H., On Waves in an Elastic Plate, *Proc. Roy. Soc. London, Ser. A 93*, pp. 114–128, 1917.

[31] Lamb, H., On the Vibrations of an Elastic Plate in Contact With Water, *Proceedings of the. Royal Society, London), Ser. A*, vol. 98, pp. 205–216, 1920.

[32] Powell, J.H. and Roberts, J.H.T., On the Frequency of Vibration of Circular Diaphragms, *Proceedings of the Physical Society, (London)*, vol. 35, pp. 170–182, 1923.

[33] Southwell, R.V., On the Free Vibrations of a Uniform Circular Disc Clamped at its Center and on the Effects of Rotation, *Proceedings of the Royal Society, (London)*, 101, pp. 133–153, 1922.

[34] Robertson, R.E., Transverse Vibrations of a Free Circular Plate Carrying Concentrated Mass, *J. App1. Mech.*, Vol. 18, no. 3, pp. 280–282, 1951.

[35] Robertson, R.E., Vibrations of a Clamped Circular Plate Carrying Concentrated Mass, *J. Appl. Mech.*, Vol. 18, No. 4, pp. 349–352, 1951.

[36] Leissa, A.W., The Free Vibration of Rectangular Plates, *J. Sound Vib., 31*, pp. 257–293,1973.

[37] Leissa, A.W.,Vibration of Plates, NASA Report SP-160, Ohio State University, Columbus, OH, 1969.

[38] Wu, J.H., Liu, A.Q. and Chen, H.L., Exact Solutions for Free-Vibration Analysis of Rectangular Plates Using Bessel Functions, *ASME, Journal of Applied Mechanics*, Vol. 74, pp. 1247–1251, 2007.

[39] Aarønes, T.E., Study of the Natural Frequencies of a Disc, MSc Thesis, EPT-M-2014-157, Norwegian University of Science and Technology, Trondheim, Norway, 2015.

[40] Savitzky, A. and Golay, M.J.E., Smoothing and Differentiation of Data by Simplified Least Squares Procedures, *Analytical Chemistry*, 36 (8), pp. 1627–1639, 1964.

[41] Acharya, D., Rani, A., Agarwal, S. and Singh, V., Application of Adaptive Savitzky—Golay Filter for EEG Signal Processing, *Elsevier, Perspectives in Science*, 8, pp. 677–679, 2016.

[42] Cleveland, R.O., and McAteer, J.A., Physics of Shock-Wave Lithotripsy, *Smith's Textbook of Endourology,* 3^{rd} *Edition*, Vol. 1, Wiley-Blackwell, pp. 527–558, 2012.

[43] Cronin, D.S. and Falzon, C., Characterization of 10% Ballistic Gelatin to Evaluate Temperature, Aging and Strain Rate Effects, *Journal of Experimental Mechanics, 51*, pp. 1197–1206, 2011.

[44] Winter, J. and Shifler, D., The Material Properties of Gelatin Gels, Ballistic Research Laboratories Report AD-A008 396, BRL Contractor Report No. 217, Ballistic Research Laboratories, Aberdeen Proving Ground, MD, 1975.

DOCUMENT CONTROL DATA

*Security markings for the title, authors, abstract and keywords must be entered when the document is sensitive

1. ORIGINATOR (Name and address of the organization preparing the document. A DRDC Centre sponsoring a contractor's report, or a tasking agency, is entered in Section 8.)

DRDC – Valcartier Research Centre
2459 de la Bravoure Road, Québec
QC G3J 1X5, Canada

2a. SECURITY MARKING (Overall security marking of the document, including supplemental markings if applicable.)

CAN UNCLASSIFIED

2b. CONTROLLED GOODS

NON-CONTROLLED GOODS
DMC A

3. TITLE (The document title and sub-title as indicated on the title page.)

On the use of the force time histories to determine the shock and steady state interface pressures exerted by the impact of a low-strength projectile

4. AUTHORS (Last name, followed by initials – ranks, titles, etc. not to be used. Use semi-colon as delimiter)

Nandlall, D.; Gakwaya, A.

5. DATE OF PUBLICATION (Month and year of publication of document.)	6a. NO. OF PAGES (Total pages, including Annexes, excluding DCD, covering and verso pages.)	6b. NO. OF REFS (Total cited in document.)
July 2018	60	44

7. DOCUMENT CATEGORY (e.g., Scientific Report, Contract Report, Scientific Letter)

Scientific Report

8. SPONSORING CENTRE (The name and address of the department project or laboratory sponsoring the research and development.)

DRDC – Valcartier Research Centre
2459 de la Bravoure Road, Québec QC G3J 1X5, Canada

9a. PROJECT OR GRANT NO. (If appropriate, the applicable research and development project or grant number under which the document was written. Please specify whether project or grant.)	9b. CONTRACT NO. (If appropriate, the applicable contract number under which the document was written.)
SOLDIER SYSTEM EFFECTIVENESS PROJECT, SoSE	

10a. DRDC DOCUMENT NUMBER	10b. OTHER DOCUMENT NO(s). (Any other numbers which may be assigned this document either by the originator or by the sponsor.)
DRDC-RDDC-2018-R161	

11a. FUTURE DISTRIBUTION WITHIN CANADA (Approval for further dissemination of the document. Security classification must also be considered.)

Public release

11b. FUTURE DISTRIBUTION OUTSIDE CANADA (Approval for further dissemination of the document. Security classification must also be considered.)

UNLIMITED

12. KEYWORDS, DESCRIPTORS or IDENTIFIERS (Use semi-colon as a delimiter.)

DRDC Scientific Report; Shock experiments; gelatine impact; gelatine shock hugoniot; bird impact; human tissue impact

13. ABSTRACT/RÉSUMÉ (When available in the document, the French version of the abstract must be included here.)

The work presented in this report examines the impact process of a 10% gelatine soft body material projectile striking a rigid target attached to a quartz force ring sensor. Using the shock Hugoniot relations and the conservations equations, a theoretical relation was obtained for the interface shock pressure. The Alekseevskii-Tate penetration equations were used to interpret and determine the steady state pressure applied to the target.

Impact tests were conducted and the time histories of the force applied to the target were measured. The force-time curves were examined to identify frequencies that were present in the results and may be coming from the natural vibrations of the various parts that make up the target. Bessel function solutions for the wave equation applied to the free vibration of plates were used to identify and quantify the frequencies of the various plates in the target assembly. These unwanted frequencies were removed using the Savitsky-Golay filter. The shock pressures were then derived and very good comparison was obtained with the theoretical values predicted by the interface shock pressure equation developed.

The Alekseevskii-Tate equation predicted very well the duration of the interaction between the projectile and the target. However, the measured value of the pressure was in discordance with the expected stagnation pressure, $P_{stagnation} = \frac{1}{2}\rho v_i^2$. In accordance with the Alexseevskii-Tate equation, the results indicate the presence of a dynamic pressure that maybe playing a significant role in the applied steady state pressure. A quantitative measure of this dynamic pressure was obtained.

L'étude présentée dans ce rapport examine le processus d'impact d'un projectile composé d'un matériel mou de 10% gélatine qui frappe une cible rigide attaché à un capteur de force annulaire. En utilisant les rapports de choc Hugoniot et les équations de conservation, une relation théorique de pression de choc a été obtenue à l'interface entre le projectile et la cible. Les équations de pénétrations d'Alekseevskii-Tate ont été utilisées pour déterminer la pression stationnaire appliquée sur la cible.

Des tests d'impact ont été effectués et les courbes de variation de force contre le temps appliqué sur la cible ont été obtenues. Ces courbes ont été examinés afin d'identifier des fréquences présentes dans les signaux et il est fort probable que ces fréquences naturelles peuvent provenir des différentes parties dont la cible est composée. Les solutions de fonctions Bessel pour l'équation d'onde appliquée à la vibration libre des plaques ont été utilisées pour identifier et déterminer quantitativement les fréquences des différentes plaques dont la cible est composée. Ces fréquences indésirables ont été enlevées en utilisant le filtre Savitsky-Golay. Subséquemment les pressions du choc ont été dérivées et une bonne comparaison avec les valeurs théoriques a été obtenues.

L'équation d'Alekseevskii-Tate a très bien prédit la durée de l'interaction entre le projectile et la cible. Cependant, le valeur de la pression a été en désaccord avec la pression de stagnation $P_{stagnation} = \frac{1}{2}\rho v_i^2$, anticipée. En interprétant les résultats selon les équations d'Alekseevskii-Tate, ces résultats indiquent la présence d'une pression dynamique qui jouerait un rôle signifiant dans la pression de l'état d'équilibre appliquée. Une mesure quantitative de cette pression dynamique a été obtenue.